



---

## THESES

préparée et présentée à

L'UNIVERSITÉ DE PAU ET DES PAYS DE L'ADOUR

pour obtenir le grade de

***Docteur***

Spécialité : CHIMIE PHYSIQUE

par

**Patricia Guevara Level**

Sujet de la thèse :

---

**Title in English**  
***Titre en français***

---

Directeur de Thèse: **Pr Didier BÉGUÉ**

Soutenue le XXth, 2016

devant la commission d'examen composée de :

### JURY

Dr Christophe RAYNAUD	Université de Montpellier, France	Rapporteur
Dr Johannes GIERSCHNER	IMDEA, Spain	Rapporteur
Dr	A	Examinateur
Dr Brigitte PEPIN-DONAT	CNRS, France	Président





# Table of Contents

<b>1 Phonon calculation</b>	<b>5</b>
1.1 Calculation of vibrational spectra of Tetracene and Pentacene Monomers: Comparison with experimental data . . . . .	6
1.1.1 Experimental data . . . . .	6
1.1.2 Computational details: construction of the potential energy surface . . . . .	7
1.1.3 Geometrical parameters of isolated tetracene molecule optimized using B3LYP and $\omega$ B97X-D methods associated with 6-311G and 6-311G** basis set . . . . .	8
1.1.4 Truncation of the potential energy surface . . . . .	9
1.1.5 Resolution of the vibrational Schrödinger equation (non-core bands with intensity) . . . . .	11
1.2 Calculation of vibrational spectra of acene dimers: Comparison with experimental data. . . . .	15
1.2.1 Calculated geometry and wavenumbers of dimers and comparison with experimental data . . . . .	16
1.2.2 $\pi$ -stacking in the acene family . . . . .	19
1.2.3 The impact of molecule distortion on the vibration modes of acene dimers	21
1.2.4 Identification of unassigned peaks in the experimental spectra of tetracene and pentacene . . . . .	23
1.3 Normal Vibrational Modes in Crystals . . . . .	26
<b>Appendices</b>	<b>55</b>



# List of Figures

1.1	Representation of a tetracene molecule.	8
1.2	Far-infrared PA spectra of (a) tetracene; (b) pentacene	12
1.3	The deformed dihedral angle C <sub>1</sub> -C <sub>2</sub> -C <sub>3</sub> -C <sub>4</sub> in Tetracene molecule	14
1.4	Comparison of theoretical and experimental wavenumbers of tetracene and pentacene	15
1.5	Optimized geometries for naphthalene dimers	17
1.6	Acene dimers in the parallel displaced configuration	20
1.7	Comparison of theoretical intramolecular vibration modes for acenes dimers . . .	22
1.8	Comparison of theoretical intermolecular vibration modes for acenes dimers . . .	23
1.9	Final assignment of the experimental infrared transitions for tetracene and pentacene	25
1.10	The <i>ac</i> and <i>ab</i> planes of benzene crystal	30
1.11	The <i>ac</i> and <i>ab</i> planes of Naphthalene crystal	31
1.12	The <i>qc</i> and <i>ab</i> planes of anthracene crystal	32
1.13	The <i>ac</i> , <i>ab</i> planes of pentacene polymorph C at the top and <i>bc</i> plane of pentacene polymorph H at the bottom	32
1.14	The <i>ac</i> and <i>ab</i> planes of phenanthrene crystal	34
1.15	The <i>ac</i> and <i>ab</i> planes of pyrene crystal	34
1.16	The <i>ac</i> and <i>ab</i> planes of Chrysene crystal	35
1.17	The <i>ac</i> and <i>bc</i> planes of Perylene crystal	36
1.18	The <i>ab</i> and <i>ac</i> planes of fluorene crystal	36
1.19	The <i>bc</i> and <i>ab</i> planes of Carbazole crystal	37
1.20	The <i>ac</i> and <i>bc</i> planes of Dibenzofuran crystal	38
1.21	The <i>ac</i> plane and other view of molecular arrangement of Dibenzothiophene crystal	38
1.22	Geometrical data for a tetracene molecule	53
1.23	Effect of mode truncature on the first ten mode on wavenumber of tetracene . .	54



# List of Tables

1.1	Method and Basis set dependence of C-C bond length ( $\text{\AA}$ ) <sup>a</sup> for tetracene monomer, and mean deviation from experimental data <sup>b</sup> . . . . .	9
1.2	Force constant truncation and separation of low and high mode influences on the values of wavenumbers of tetracene monomer based on a force field extracted from calculations at the $\omega\text{B97X-D}/6-311\text{G}$ level of theory. . . . .	10
1.3	Experimental and calculated wavenumbers ( $\text{cm}^{-1}$ ) for fundamental and combination vibrational modes of tetracene. . . . .	12
1.4	Experimental and calculated wavenumbers ( $\text{cm}^{-1}$ ) for fundamental and combination vibrational modes for pentacene. . . . .	13
1.5	Geometry dependence of basis sets on structures PD and $\text{C}_2$ shown in Figure 4.5	17
1.6	Interaction energies in kcal/mol and associated wavenumber ( $\text{cm}^{-1}$ ) of optimized naphthalene dimers. . . . .	18
1.7	Calculated wavenumber ( $\text{cm}^{-1}$ ) of the intra- and intermolecular vibrational modes of the naphthalene dimer in the configuration a) and b) at the $\omega\text{B97X-D}/6311\text{G}$ level with BSSE-correction, compared with frequencies obtained at the MP2/cc-pVDZ level in the article of Saeki et al[1]. . . . .	19
1.8	Intermolecular distance and Interaction energies calculated for acene dimers. . . . .	21
1.9	Calculated intermolecular vibrational modes ( $\text{cm}^{-1}$ ) and their intensities for naphthalene, anthracene, tetracene and pentacene dimers. . . . .	21
1.10	Intramolecular vibration modes ( $\text{cm}^{-1}$ ) and the corresponding intensities in brackets (km/mol) for naphthalene, anthracene, tetracene and pentacene dimers. Values of corresponding monomer modes are written below in italics. . . . .	24
1.11	Interaction energies calculated for distorted acene dimers. . . . .	25
1.12	Calculated intermolecular vibrational modes ( $\text{cm}^{-1}$ ) and their intensities for distorted dimers of naphthalene, anthracene and tetracene. . . . .	26
1.13	Lattice parameters of Tetracene molecule calculated in VASP code . . . . .	27
1.14	Calculated vibrational frequencies ( $\text{cm}^{-1}$ ) of the monomer, dimer and solid-state (PBE tetracene system). . . . .	29
1.15	Lattice parameters of benzene molecule calculated in VASP code . . . . .	31
1.16	Lattice parameters of naphthalene molecule calculated in VASP code . . . . .	31
1.17	Lattice parameters of anthracene molecule calculated in VASP code . . . . .	32
1.18	Lattice parameters of Pentacene molecule (Polymorphe H) calculated in VASP code . . . . .	33
1.19	Lattice parameters of pentacene molecule (polymorphe C) calculated in VASP code . . . . .	33
1.20	Lattice parameters of phenanthrene molecule calculated in VASP code . . . . .	34
1.21	Lattice parameters of pyrene molecule calculated in VASP code . . . . .	35

1.22 Lattice parameters of chrysene molecule calculated in VASP code . . . . .	35
1.23 Lattice parameters of Perylene molecule calculated in VASP code . . . . .	36
1.24 Lattice parameters of Fluorene molecule calculated in VASP code . . . . .	37
1.25 Lattice parameters of Carbazole molecule calculated in VASP code . . . . .	37
1.26 Lattice parameters of Dibenzofuran molecule calculated in VASP code . . . . .	38
1.27 Lattice parameters of Dibenzothiophene molecule calculated in VASP code . . . . .	39
1.28 Calculated vibrational frequencies ( $\text{cm}^{-1}$ ) of the monomer, dimer and solid-state (PBE Benzene system). . . . .	39
1.29 Calculated vibrational frequencies ( $\text{cm}^{-1}$ ) of the monomer, dimer and solid-state (PBE Naphthalene system). . . . .	40
1.30 Calculated vibrational frequencies ( $\text{cm}^{-1}$ ) of the monomer, dimer and solid-state (PBE Anthracene system). . . . .	41
1.31 Calculated vibrational frequencies ( $\text{cm}^{-1}$ ) of the monomer, dimer and solid-state (PBE Pentacene system). . . . .	42
1.32 Calculated vibrational frequencies ( $\text{cm}^{-1}$ ) of the monomer, dimer and solid-state (PBE Phenanthrene system). . . . .	43
1.33 Calculated vibrational frequencies ( $\text{cm}^{-1}$ ) of the monomer, dimer and solid-state (PBE Pyrene system). . . . .	44
1.34 Calculated vibrational frequencies ( $\text{cm}^{-1}$ ) of the monomer, dimer and solid-state (PBE Chrysene system). . . . .	45
1.35 Calculated vibrational frequencies ( $\text{cm}^{-1}$ ) of the monomer, dimer and solid-state (PBE Perylene system). . . . .	46
1.36 Calculated vibrational frequencies ( $\text{cm}^{-1}$ ) of the monomer, dimer and solid-state (PBE Fluorene system). . . . .	47
1.37 Calculated vibrational frequencies ( $\text{cm}^{-1}$ ) of the monomer, dimer and solid-state (PBE Carbazole system). . . . .	48
1.38 Calculated vibrational frequencies ( $\text{cm}^{-1}$ ) of the monomer, dimer and solid-state (PBE Dibenzofuran system). . . . .	49
1.39 Calculated vibrational frequencies ( $\text{cm}^{-1}$ ) of the monomer, dimer and solid-state (PBE Dibenzothiophene system). . . . .	50
1.40 Computed wavenumbers and intensities for distorted tetracene based on the harmonic approximation at the $\omega\text{B97X-D}/6-311\text{G}$ level of calculation. Comparison with symmetric tetracene ( $\text{D}_{2h}$ ) . . . . .	54

# **Chapter 1**

## **Acenes**

# Introduction

The strategy in the present work is to perform high-precision quantum mechanical calculations based on harmonic and anharmonic electrical and mechanical approximations to compute spectra for individual molecules, dimers and for systems in solid state. The detailed identification of bands in experimental vibration spectra for crude oils and oil fractions may eventually permit the identification of the presence of members of a family of molecules, and the determination of the significance of specific types of molecular interaction arising in these fluids through spectral decomposition. Potential impacts include: improved speciation, and hence fluid characterization; and improved understanding of association phenomena, such as  $\pi - \pi$  interactions, and hence transport property prediction.

Acenes, a family of linear polynuclear aromatic compounds possessing only  $\pi - \pi$  interactions, for which high precision experimental data are available up to pentacene [2], comprise a first benchmark example that illustrates both the potential and the computational challenges found in this line of inquiry. In this respect, various calculation hypotheses used for these large molecules are presented, together with the impact of these calculation hypotheses on the quality vis-à-vis experimental data and the computational cost of vibrational spectra.

Spectral assignments, determined on the basis of both wavenumber and relative intensity values, are made primarily using computed spectra for individual molecules, and dimers. In addition, based on experimental observation assessing the presence of deformed molecules in tetracene and pentacene crystals, impact on vibrational spectra of these deformations is evaluated. Finally, the phonon spectra of the two tetracene and pentacene systems are calculated in order to finalize assignments and to calibrate our methodological approaches.

In the last part of this chapter additional calculations were performed for other compounds of the acene family, as well as other systems of the aromatic polycycle molecules family. The aim of these additional calculations is verifying if the position and activity of the network modes identified for the two tetracene and pentacene molecules in the solid state, and particularly the more active mode, depend on the size, length or on the moiety of the polycycle system in study.

## 1.1 Calculation of vibrational spectra of Tetracene and Pentacene Monomers: Comparison with experimental data

### 1.1.1 Experimental data

Experimental solid-state infrared spectra of tetracene and pentacene [2] were acquired at room pressure and temperature. The measurements were performed on as received samples. Thus the crystallinity as well as the possible presence of defects in these solids are unknown. For tetracene, two crystal structures have been detected by x-ray diffraction experiments [3]. At room temperature and pressure, tetracene is triclinic [4] with space group  $P\bar{1}$ . The unit cell contains two independent molecules at the  $(0, 0, 0)$  and  $(1/2, 1/2, 0)$  inversion sites. Pentacene possesses two polymorphs [5, 6]. One comprises a triclinic layered structure with a herringbone arrangement in the layers, with two equivalent molecules per unit cell [5]. The other, commonly

found at room temperature, adopts a 14.1 Å d(001)-spacing morphology with an inversion center on both molecules in the unit cell [7, 8, 6, 9, 10].

### 1.1.2 Computational details: construction of the potential energy surface

The Becke Three-Parameters Hybrid Functional (B3LYP), a combination of the Becke three-parameter exchange functional (B3) [11] that includes a mixture of Hartree-Fock exchange with the density functional theory (DFT) exchange-correlation and the LYP correlation functional [12], has proven to be a reasonable choice for predicting geometries of aromatic molecules [13, 14]. Stephens et al. [15] showed that the B3LYP force field yields infrared spectra in very good agreement with experimental data. It has become a standard method for studying vibrational spectra of organic molecules (in the far- and mid- Infrared) in the gas phase [16, 17]. Although the B3LYP method coupled with a sufficiently large basis set is a good candidate to study vibrational spectra of polynuclear aromatic molecules [2], this standard DFT calculation approach fails to describe long-distance interactions. Consequently, it does not reproduce spectra of interacting molecules [11, 15, 18, 19] where the interpretation of experimental vibration spectra requires consideration of both isolated and interacting molecules.

In parallel to the development to ab initio methods, some progress has been made on implementing the London dispersion force effect into DFT methods, permitting calculations with larger individual molecules and binary pairs. Although the CCSD(T) method in combination with a sufficiently flexible basis set is the most accurate method for reproducing rotation-vibration spectra and to describe intermolecular complexes between aromatic hydrocarbons [20], such calculations are impractical for the description of large molecules [21]. The MP2 method [22], also able to handle dispersive interactions such as  $\pi - \pi$  stacking [23, 24], is a computationally intensive and inadequate method for large molecules too [25]. Chai et al. [26] developed a functional based on optimized long-range corrected hybrid density functionals [26], which employs 100% Hartree-Fock (HF) exchange for long-range electron-electron interactions,  $\omega$ B97X, to which they added an empirical dispersive interaction correction [?]. This method was tested by Salzner et al [27] for  $\pi$ -conjugated oligomers and it overcame the difficulties encountered with standard DFT functionals when dealing with interacting  $\pi$ -systems.

In this work, for isolated molecules and dimers, extended basis-sets consisting of atomic orbitals expressed as fixed linear combinations of Gaussian functions are employed for the calculations. A split valence 6-311G and 6-311G(p,d) [28, 29] was needed to provide correct calculation outcomes for naphthalene monomer [1]. Validation tests for the  $\omega$ B97X-D/6-311G calculation method were also performed. The accuracy of DFT calculations in predicting molecular geometries and vibrational frequencies depend on the density functional employed. Thus geometrical optimizations were performed for isolated tetracene, using the  $\omega$ B97X-D functional as well as the more conventional B3LYP method. The computational results are benchmarked using experimental data obtained by Campbell et al.[4].

The solid state calculations in the present work were carried out with the use of two approaches: First, the calculations were carried out with the projector augmented wave (PAW) implementation of Vienna Ab initio Simulation Package (VASP)[30]. The generalized gradient approximation (GGA) in the PBE parameterization was considered as the exchange corre-

tional functional [31]. Structural optimizations (triclinic tetracene crystal) were achieved by setting the convergence criteria for total energies below  $5 * 10^{-6}$  eV, residual forces to be less than  $1 * 10^{-3}$  eV/Å, and stresses limited to 0.02 GPa. To correct the missing dispersion interactions, we have used several recently proposed methods such as PBE functional with pair potential methods D2, D3 (BJ), TS, and TS+SCS. The details of the implementations and usage of these methods can be found elsewhere [32, 33, 34, 35, 36]. To obtain accurate band gaps, we have used the GW approximation<sup>86</sup>. For getting accurate quasiparticle eigenvalues, we used 200 bands for the summation over the bands in the polarizability and the self-energy formulas, and the polarizability matrices were calculated up to a cutoff of 200 eV.

Second, periodic calculations for tetracene were also performed in order to calculate IR intensities with CRYSTAL14 program[37], using PBE functional and STO-6G (Pople's STO-6G) basis set. Default criteria were used as consider accuracy and SCF convergence. Vibrational frequencies at the  $\Gamma$  Point were calculated for the optimized geometry. The empirical dispersion correction by Grimme [32] was performed to take into account weak interactions.

### 1.1.3 Geometrical parameters of isolated tetracene molecule optimized using B3LYP and $\omega$ B97X-D methods associated with 6-311G and 6-311G\*\* basis set

Geometry optimizations were performed using two different DFT methods (B3LYP and  $\omega$ B97X-D) implemented in Gaussian 09 software [38], and two basis sets (6-311G and 6-311G\*\*). While Saeki et al. [1] reported a change of symmetry for the naphthalene molecule, from  $D_2h$  to  $C_2h$  (based on MP2/6-311G calculations), optimized geometries for the tetracene molecule, which also possesses  $D_2h$  symmetry, remained planar with  $D_2h$  symmetry in all cases. Calculated bond lengths based on different levels of theory are listed in Table 1 along with their mean deviations from experimental measurements (see also Figure A1 in the supplementary data). For these calculations, irrespective of the level of theory or the basis set employed, the agreement between computed bond lengths and experimental values is very good. The mean deviation from experimental values is less than 0.03 Å. These results show clearly that the choice of calculation method and basis set has a minor influence on the geometry of tetracene. Results obtained with pentacene monomer are comparable. This basis-set insensitivity for DFT approaches has been illustrated previously[39]. It permits the use of smaller basis sets and provides an additional argument for the use of DFT over ab initio methods, since larger molecules can be treated. The  $\omega$ B97X-D method, which contains a London-force dispersive term, and is reliable for acene molecules was selected for this study and it is used in combination with the 6-311G basis-set.

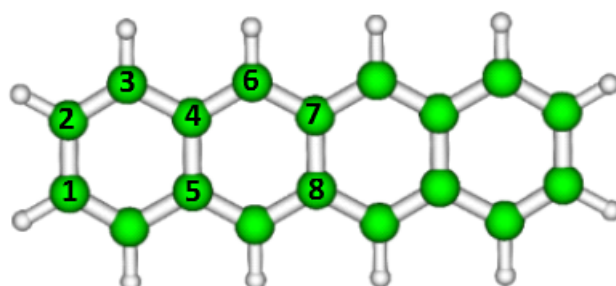


Figure 1.1 – Representation of a tetracene molecule.

Table 1.1 – Method and Basis set dependence of C-C bond length ( $\text{\AA}$ )<sup>a</sup> for tetracene monomer, and mean deviation from experimental data<sup>b</sup>

	$C_1 - C_2$	$C_2 - C_3$	$C_3 - C_4$	$C_4 - C_5$	$C_5 - C_6$	$C_6 - C_7$	$C_7 - C_8$	Mean deviation
Experimental data <sup>a</sup>	1.46	1.38	1.42	1.42	1.39	1.40	1.46	
B3LYP/6-311G	1.43 (-0.03)	1.36 (-0.02)	1.43 (+0.01)	1.43 (+0.01)	1.40 (+0.01)	1.42 (+0.02)	1.43 (-0.03)	0.02
B3LYP/6-311G**	1.43 (-0.03)	1.36 (-0.02)	1.43 (+0.01)	1.43 (+0.01)	1.40 (+0.01)	1.42 (+0.02)	1.43 (-0.03)	0.03
$\omega$ B97X-D/6-311G	1.43 (-0.03)	1.37 (-0.02)	1.44 (+0.02)	1.45 (+0.03)	1.39 (=)	1.41 (+0.01)	1.45 (-0.01)	0.02
$\omega$ B97X-D/6-311G**	1.43 (-0.03)	1.37 (-0.02)	1.44 (+0.02)	1.45 (+0.02)	1.39 (=)	1.41 (+0.01)	1.45 (-0.01)	0.02

<sup>a</sup> The values in parenthesis indicate the difference between the calculated and experimental bond lengths.

<sup>b</sup> Experimental bond lengths are obtained from ref[4].

### 1.1.4 Truncation of the potential energy surface

Vibrational spectroscopy modelling outcomes, whether at the harmonic or anharmonic level, are directly dependent on the quality of the potential energy surface (PES). The PES is generally expressed as a polynomial determined by adjustment of a set of geometric structures of a molecule. Consequently this type of calculation depends on the quality of the electronic calculations of the wave functions as well. While it is now common to determine the PES accurately for small molecules (3-5 atoms) [40], this becomes almost infeasible when solving anharmonic approximations for systems of larger size where powerful computers are required to implement rigorous methods for solving the Schrödinger equation. Truncation of the analytical shape of the PES (degree of the potential), is unavoidable. For example, a tetracene molecule contains 30 atoms, and therefore has  $3N - 6 = 84$  normal modes apart from the translational and rotational modes. 84 modes with an order 4 necessitates the calculation for 22171 force constants. Thus, truncation of the PES constitutes the first part of this study. Four levels of approximation were tested. The fundamental bands obtained in these cases, using second-order perturbation theory (PT2), are compared to the ones calculated with the complete PES. The conclusion of these tests are summarized in Table 1.2 and elaborated here:

1. It is possible to truncate the PES in terms of only significant coupling. For this, it suffices to identify the constant of cubic and quartic force of very low intensity. We have realized calculations by successively suppressing force constants smaller than 2, 5, 8 and  $10 \text{ cm}^{-1}$ . This study showed that the discrepancy regarding the calculated frequencies of fundamental modes is not higher than  $2.8 \text{ cm}^{-1}$ , and  $3.3 \text{ cm}^{-1}$  for the combination modes. These disparities are small enough to justify use of this approximation. Moreover this allows setting 7, 33, 48 and 55 % of the forces to zero when suppressing constants smaller than 2, 5, 8 and  $10 \text{ cm}^{-1}$ , respectively, thus saving computational cost and enabling variational calculations for larger systems. Note, however, that this restriction is potentially acceptable only without any Fermi or Darling-Dennison resonance, often characterized totally or partially using these finest couplings. Regarding the time saved when suppressing the forces lower than  $10 \text{ cm}^{-1}$  while the wavenumber values of fundamental modes remain the same, it would be tempting to truncate the PES this way, but this would represent a serious risk of losing information regarding combination bands. Indeed

Table 1.2 – Force constant truncation and separation of low and high mode influences on the values of wavenumbers of tetracene monomer based on a force field extracted from calculations at the  $\omega$ B97X-D/6-311G level of theory.

Polynomial degree	2	$4^c$	$4^c$	$4^c$	$4^c$	$6^c$
Force constants (f) considered		All f considered	$f > 5 \text{ cm}^{-1}$	$f > 5 \text{ cm}^{-1}$	$f > 5 \text{ cm}^{-1}$	All f considered
Number of modes	84	84	84	20	10	10
Mode (symmetry)	Exp. values <sup>a</sup>					
$\nu_1(B_{3u})$	57	48	53	62	60	69
$\nu_2(A_u)$	93	90	96	107	103	107
$\nu_3(B_{1g})$	154	150	154	161	160	164
$\nu_4(B_{1u})$	166 <sup>b</sup>	168	169	160	169	171
$\nu_5(B_{2g})$	196	194	200	204	202	203
$\nu_6(B_{3u})$	271 <sup>b</sup>	276	272	277	284	282
$\nu_7(B_{3g})$	316	317	305	317	317	319
$\nu_8(A_g)$	322 <sup>b</sup>	324	322	323	322	320
$\nu_9(A_u)$	327	325	332	330	328	331
$\nu_{10}(B_{1g})$	389	382	386	395	392	394

<sup>a</sup> Experimental values of wavenumbers are obtained from ref[2].

<sup>b</sup> Experimental uncertainty equal to +/- 2  $\text{cm}^{-1}$ .

<sup>c</sup> Wavenumbers calculated using second-order perturbation theory (PT2)

our tests show that the upper limit of the truncation to maintain all the information of combination bands consists in considering all the forces higher than  $5 \text{ cm}^{-1}$ . Removal of these forces would disregard combinations whose weight is less important, resulting in the loss of details that provide a complete interpretation of infrared spectra. Thus, for the following tests of truncature and for calculations presented in this study, we will consider a PES calculated with force constants higher than  $5 \text{ cm}^{-1}$ .

2. The second truncation tested in this work consists of separating modes of high and low wavenumber. We assumed that the description of the low-wavenumber modes (mainly torsion modes), were weakly coupled with bending and scissoring modes occurring at higher wavenumber. This hypothesis has been tested and validated on the base of calculations on the tetracene molecule (Table 2); indeed each of the first 15 modes calculated using the PES truncated to torsional and libration modes are in perfect adequacy with values calculated a posteriori using complete PES.
3. We have also tested the association of a complete grid of points of the surface at the fourth order, with a fit at the sixth order on the diagonal, in order to refine coupling between closely coupled modes. Because this refining is demanding in terms of computing time,

we applied it on the 10 first modes only, supposing that the modes of higher wavenumber were correctly described with a polynome of 4<sup>th</sup> order. The results, listed in Table 2, show that this refining doesn't bring any improvement for describing the vibrational spectrum of tetracene.

4. The last approximation used in this work consists of applying a second adjustment of the PES; this adjustment would aim to eliminate the weight of vibrators we excluded in point (i), to refine the fit of remaining force constants so that they reflect, in fine, only the couplings between remaining modes. If this had proved to be an acceptable approximation, we could have extended this methodology to the study of specific molecules vibrators of undifferentiated dimension, by calculating a limited number of specific points to sought vibrators. In accordance with what Bowman et al [41] and Begue et al [42] showed on the study of water clusters, our calculations show that only the separation between libration modes with all other active modes is possible.

To conclude, we have shown that partial truncation of PES could be effective for our study. This truncation consists of extracting from a global fit, the force constants of higher order that allow the description of the problem beyond the harmonic approximation. These constants can then be directly used to solve Schrödinger's vibrational equation.

This methodology was used in the remainder of our work for the characterization and assignment of the spectra of tetracene and pentacene molecules.

### 1.1.5 Resolution of the vibrational Schrödinger equation (non-core bands with intensity)

The presence of overtones and combination bands in infrared spectra is a manifestation of the breakdown of the double-harmonic approximation, usually implemented in electronic structure codes. The calculation of intensities is essential in order to determine which non-fundamental transitions are active and to assign all experimental bands. Since both mechanical (anharmonicity of the potential) and electrical (non-linear dependence of the dipole moment on the normal coordinates) anharmonicities are expected to give non-zero intensities to non-fundamental transitions, these two effects must be considered in the treatment of transition energies and related vibrational wavefunctions. The wavenumber calculations in the mechanical anharmonic approximation were carried out using a variational method developed by Bégué et al [40]. Using this method, implemented in the P\_Anhar.v2.0 program [43], it was possible to compute all the vibrational frequencies (fundamental, combination bands and overtones) that contribute to the mid- and near-infrared spectrum of tetracene and pentacene. In addition, the activity of each mode was also calculated in the electrical anharmonic approximation using a method developed by Baraille et al [42, 44], which is also available in the same software.

The experimental spectra of tetracene and pentacene, extracted from the work of Michaelian et al [2], are shown in Figure 1.2. The corresponding calculated infrared active transitions both fundamental and combination bands overlay the data and are listed in Table 1.3 and Table 1.4 where they are further compared with available experimental and theoretical values. Threshold intensity for IR-activity of 0.001 km/mol was chosen for the calculations. This threshold is justified following a discussion of band assignments for each molecule, and presentation of vibrational bands common for the two molecules.

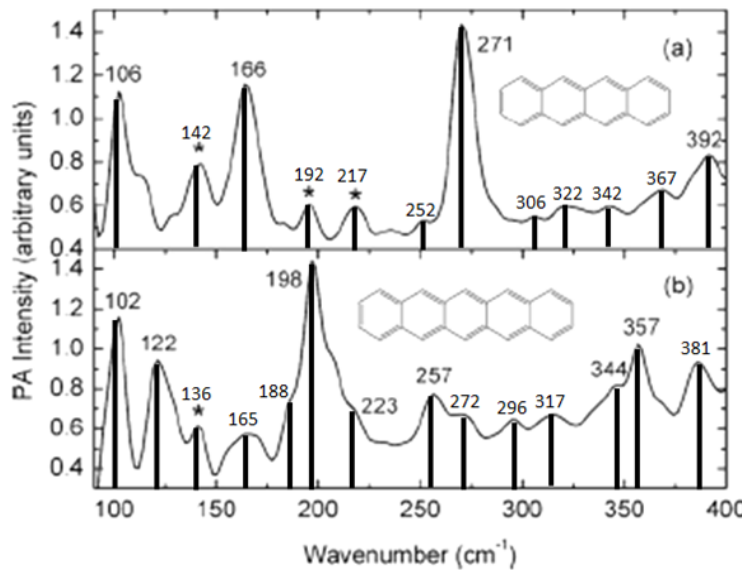


Figure 1.2 – Far-infrared PA spectra of (a) tetracene; (b) pentacene. Spectra were acquired using phase modulation at a frequency of 5 Hz and an amplitude of  $15 \lambda$  ( $\lambda = 0.6328 \mu m$ ), extracted from Michaelian et al [2]

Table 1.3 – Experimental and calculated wavenumbers ( $\text{cm}^{-1}$ ) for fundamental and combination vibrational modes of tetracene.

Mode	Type of vibration	Symmetry	Experimental values			Predicted bands		Theoretical IR Intensity <sup>a</sup> km/mol
			Michaelian et al[2]	Michaelian et al[2]	Cataldo et al[45]	Harmonic $\text{cm}^{-1}$	Anharm (PT2) $\text{cm}^{-1}$	
$\nu_3$	Wagging	$B_{1g}$	106(m)			154R <sup>c</sup>	153R <sup>c</sup>	0.01 <sup>b</sup>
$3\nu_1$		$B_{3u}$	142(m)				132	0.003
$\nu_4$	Scissoring	$B_{1u}$	166(s)	$B_{1u}$	166	160	168	1.3
$\nu_5$	Wagging	$B_{2g}$	197(w)			196R <sup>c</sup>	199R <sup>c</sup>	0.05 <sup>b</sup>
$\nu_1 + \nu_3$		$B_{2u}$					201	0.005
$\nu_1 + 2\nu_2$		$B_{3u}$	217(w)				228	0.001
$\nu_2 + \nu_3$		$B_{1u}$	252(vw)				247	0.002
$\nu_6$	Wagging	$B_{3u}$	271(m)	$B_{3u}$	278	266	276	1.03
$\nu_2 + \nu_5$		$B_{2u}$	306(vw)				293	0.002
$\nu_8$	Stretching	$A_g$	322(w)			324R <sup>c</sup>	322R <sup>c</sup>	0.002 <sup>b</sup>
$\nu_1 + 2\nu_3$		$B_{3u}$	342(w)				353	0.003
$\nu_1 + \nu_8$		$B_{3u}$	367(m)				379	0.003
$\nu_{10}$	Alternate wagging	$B_{1g}$	392(m)	$B_{1g}$	388R	374R	389R	0.04 <sup>b</sup>
$2\nu_1 + \nu_6$		$B_{3u}$					380	0.004

<sup>a</sup> Theoretical intensities obtained using perturbational-variational calculations, with truncated potential on the 20 first modes. <sup>b</sup> Theoretical intensities obtained for the distorted molecule, at the harmonic level. <sup>c</sup> The letter R indicates Raman-active modes.

For tetracene molecules, three bands were identified previously in the range 100 – 400 cm<sup>-1</sup> [2, 46]. Two were noted as infrared active at 166 and 271 cm<sup>-1</sup>, and one (388 cm<sup>-1</sup>) was assigned as Raman-active (Table 1.3). By calculating intensities for all bands, including combination bands and overtones, 8 additional infrared- active vibrations (7 combinations and one second-harmonic) are identified, and the band at 388 cm<sup>-1</sup> previously assigned as Raman-active is identified as an infrared-active band arising from the B3u mode plus an overtone. Three similar cases where a vibrational transition could correspond either to a combination band, an overtone, or a Raman-active band, are also shown in Table 1.3.

Table 1.4 – Experimental and calculated wavenumbers (cm-1) for fundamental and combination vibrational modes for pentacene.

Mode	Type of vibration	Symmetry	Experimental values			Predicted bands		Theoretical IR Intensity <sup>a</sup> km/mol
			Michaelian et al[2]	Michaelian et al[2]	Cataldo et al[45]	Harmonic cm <sup>-1</sup>	Anharm (PT2) cm <sup>-1</sup>	
$\nu_3$	Wagging	B <sub>1g</sub>	102(m)	B <sub>1g</sub> 105R <sup>c</sup>	100R <sup>c</sup>	104R <sup>c</sup>	97R <sup>c</sup>	0.003 <sup>b</sup>
$\nu_4$	Scissoring	B <sub>1u</sub>	122(m)	B <sub>1u</sub> 121	117	123	122	1.0
$\nu_1 + \nu_3$		B <sub>2u</sub>	141(m)				144	0.004
$\nu_2 + \nu_3$		B <sub>1u</sub>	165(vw)				164	0.0005
$\nu_6$	Wagging	B <sub>3u</sub>	198(m)	B <sub>3u</sub> 198	189	198	194	1.4
$\nu_3 + \nu_4$		A <sub>u</sub>	223(vw)				224	0.0
$\nu_2 + \nu_5$		B <sub>2u</sub>					222	0.002
$\nu_9$	Symmetric stretching	A <sub>g</sub>	257(w)	A <sub>g</sub> 266R <sup>c</sup>	258R <sup>c</sup>	269R <sup>c</sup>	265R <sup>c</sup>	0.0 <sup>b</sup>
$\nu_1 + 2\nu_3$		B <sub>3u</sub>					251	0.0006
$2\nu_1 + \nu_6$		B <sub>3u</sub>	272(vw)				274	0.0007
$\nu_3 + \nu_6$		B <sub>2u</sub>	296(w)				291	0.003
$\nu_1 + \nu_9$		B <sub>3u</sub>					292	0.003
$\nu_2 + \nu_7$		B <sub>3u</sub>	317(w)				316	0.0009
$\nu_3 + \nu_8$		B <sub>1u</sub>	344(vw)				346	0.03
$\nu_{12}$	Scissoring	B <sub>1u</sub>	357(w)	B <sub>1u</sub> 369	357	375	374	0.1
$\nu_{13}$	Alternate wagging	B <sub>3u</sub>	381(m)			385	374	0.03

<sup>a</sup> Theoretical intensities obtained using perturbational-variational calculations, with truncated potential on the 20 first modes.    <sup>b</sup> Theoretical intensities obtained for the distorted molecule, at the harmonic level.    <sup>c</sup> The letter R indicates Raman-active modes.

## Raman-transition active in infrared: molecular deformation

Raman transitions can become active in infrared spectre, when a molecule is deformed in the solid state. For example, Homes et al[7] showed experimentally that acene molecules in the solid state are not planar and attributed this observation to crystal-packing forces that induce deformation; additionally, deformation effect on lattice-phonon frequencies has been measured, then enabling discrimination of different solid phases of tetracene [3] and pentacene [47, 48]. In order to underpin this contention, we performed calculations on a deformed tetracene molecule, shown in Figure 1.3. In this conformation the molecule does not possess D<sub>2h</sub> symmetry. The molecule does still possess symmetry, however. The deformation concerns dihedral angles [C<sub>1</sub>-

$C_2-C_3-C_4]$ ,  $[C_2-C_3-C_4-C_5]$ ,  $[C_4-C_5-C_6-C_7]$ ,  $[C_5-C_6-C_7-C_8]$ ,  $[C_9-C_{10}-C_{11}-C_{12}]$  and  $[C_{10}-C_{11}-C_{12}-C_{13}]$ , equal to  $175^\circ$ ,  $178^\circ$ ,  $-178^\circ$ ,  $-178^\circ$ ,  $-178^\circ$ , respectively, instead of  $\pm 180^\circ$  in the case of the molecule in the D<sub>2h</sub> conformation. The bond lengths are unchanged. Wavenumbers of fundamental modes and associated intensities calculated with the harmonic approximation are listed in Table A1 in the supplementary data. The calculated vibrational spectrum exhibits only positive wavenumbers, which attests that this deformation is located at a minimum of the PES. The intensities corresponding to the R-denominated-bands of the deformed molecule, calculated at the harmonic level, are given in Table 1.3. For the deformed molecule, modes that would normally be inactive in infrared (Raman active or silent modes), present significant intensities, ranging from 0.002 to 0.05 km/mol.

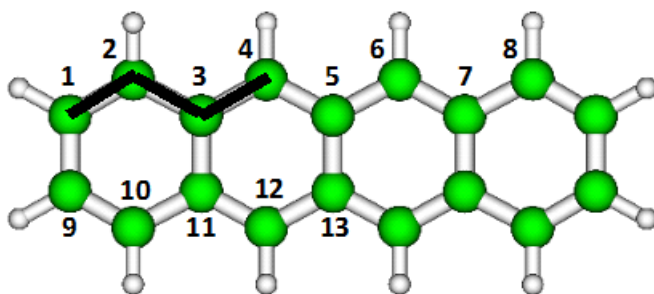


Figure 1.3 – Tetracene molecule. The deformed dihedral angle  $C_1-C_2-C_3-C_4$  is shown in black.

## Assignment based on intensity value

Transitions for which there is a double hypothesis ( $142$ ,  $192$  and  $392\text{ cm}^{-1}$ ) can be resolved on the basis of relative intensity values. Thus the band at  $142\text{ cm}^{-1}$  could be attributed to a second harmonic whose intensity would be three times lower than the Raman-active one that becomes optically active for the deformed molecule. The band at  $192\text{ cm}^{-1}$  could be either a combination of an IR-active mode and a Raman-active mode, whose intensity would be ten times lower than a Raman-active band calculated at  $196\text{ cm}^{-1}$ . The band at  $392\text{ cm}^{-1}$  could either be a combination of an overtone and an infrared active mode, or a Raman-active band ten times more intense. From the relative intensities, in each case, the assumption of the Raman-band becoming active is more likely. For other transitions, there is a single hypothesis. The transition, denoted  $v_8$ , located at  $322\text{ cm}^{-1}$  is a Raman-active band while the bands located at  $252$ ,  $306$  and  $342\text{ cm}^{-1}$  are combination bands.

For pentacene, Table 1.4, the situation is similar. 11 bands arise from combination vibrations. One, found experimentally at  $257\text{ cm}^{-1}$ , was previously assigned to a predicted Raman-active mode. Calculations on a deformed pentacene molecule lead to an IR active band at a comparable wavenumber and with a comparable intensity. Thus, this one assignment remains uncertain on the basis of these calculations.

## Use of trends for assignment

The trends for normal modes of infrared active vibrations found for both tetracene and pentacene molecules (see types of vibration in Table 1.3 and Table 1.4) are shown in Figure 1.4 where they are also compared with experimental data. By viewing the wavenumbers in this

way, wavenumber assignments for the two molecules can be evaluated in parallel. From the similarity of the trends for tetracene and pentacene, as well as the proximity of the respective computed wavenumbers to experimental ones, the assignment choices - combination bands over Raman-active ones – are supported and this outcome is independent of intensity values. Only one band remains unassigned in the experimental spectrum of tetracene, 106 cm<sup>-1</sup>. Michaelian et al [2] suggested that it originated from lattice vibration. The pentacene band attributed to a Raman-active vibration, 102 cm<sup>-1</sup>, may be of the same type as well. These bands and intermolecular bands more broadly are addressed by performing calculations with tetracene and pentacene dimers.

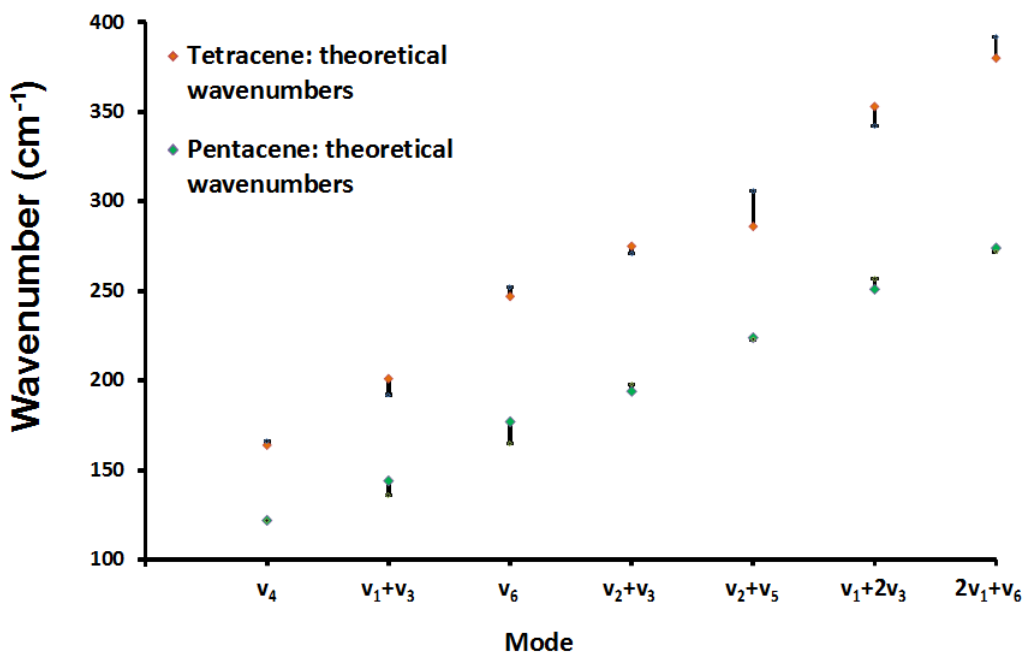


Figure 1.4 – Comparison of theoretical and experimental wavenumbers of tetracene and pentacene for the same normal modes of vibration. The deviations between experimental and theoretical wavenumbers are represented with dark bars.

## 1.2 Calculation of vibrational spectra of acene dimers: Comparison with experimental data.

$\pi$ -stacking is responsible for the cohesive structure of acene crystals [4, 6, 49, 50, 51]. Dimers constitute a benchmark for describing  $\pi$ -stacking phenomena. In order to generalize the effect of  $\pi$ -stacking on intermolecular vibrations for the acene family as a whole, the calculations described here include those for naphthalene and anthracene dimers in addition to the tetracene and pentacene dimers. Inclusion of these smaller dimers also permits calibration of the computational methodology employed.

### 1.2.1 Calculated geometry and wavenumbers of dimers and comparison with experimental data

Far-infrared spectra provide information about intermolecular and inter-ring interactions and about  $\pi$ -stacking in particular. Hineno et al [52] measured spectra of naphthalene and anthracene in the region 190-50 cm<sup>-1</sup> at liquid helium temperature and observed that some bands were due to lattice vibrations. In the same way, bands in the experimental vibrational spectra of tetracene and pentacene that cannot be interpreted based on computed wavenumbers for a single molecule are expected to arise from lattice modes. A first step toward understanding  $\pi - \pi$  interaction of acene compounds consists of considering the interaction of acene dimers. The choice of the calculation method for describing these electronic interactions is justified, and then the differentiation of inter- and intramolecular vibrations in the acene family, is addressed.

**Naphthalene dimer:** to assess the performance of the  $\omega$ B97X-D method for  $\pi - \pi$  interaction calculations involving aromatic molecules, the robustness of the  $\omega$ B97X-D/6-311G method for naphthalene dimers, for which a broad literature exists [1, 48] 50,97,98,99,100, is discussed in light of results based on reliable data and accurate computational results. For example, Gonzalez et al.102 and Tsuzuki et al [53] calculated ground-state structures and binding energies of van der Waals dimers of naphthalene using an aromatic intermolecular interaction model, at the MP2 and CCSD(T) levels of theory, respectively, using Pople's basis sets of various size. Their calculations yield two low energy dimers of similar energy: D<sub>2d</sub> (crossed) and C<sub>2h</sub> (parallel-displaced), and two C<sub>2v</sub> T-shaped structures. Walsh et al [54, 55], using calculations at the MP2/6-31\*(0.25) level found eight stationary points for naphthalene dimers: the four reported previously and four others of lower symmetry. Following these studies, Saeki et al [1] performed vibrational analysis of naphthalene dimers at the MP2/6-311G level of theory and their results are compared with the values obtained in this work. In the present work, geometry optimizations of naphthalene dimers in various configurations - parallel displaced (PD), parallel displaced according to C<sub>2h</sub> symmetry, crossed-parallel according to C<sub>2</sub> and D<sub>2h</sub> symmetry - using the  $\omega$ B97X-D method, with the 6-311G and 6-311G(p,d) basis sets were performed. All stationary points were characterized by frequency calculations to ensure that the optimized structures were located at a local minimum. The basis set superposition error (BSSE) correction developed by Simon et al.106 was included in the calculations for all complexes. Calculations without this correction were carried out to characterize the importance of this error. Negative binding energies indicate exothermic complex formation [56]. Analysis of dimer configurations showed that only the low-level symmetry configurations, C<sub>2</sub> and parallel-displaced (PD), represented in Figures 5a and b, respectively, correspond to minima on the PES. Vibrational calculations for the symmetric configurations exhibited negative frequencies. This outcome is in agreement with Walsh et al [54] who showed that structures of low symmetry are the most stable. The center of mass separation (r), rotation angle ( $\Theta$ ) for the C<sub>2</sub> structure, and the distance of relative translation (x<sub>1</sub> and x<sub>2</sub>) for the PD structure are given in Table 1.5. For these two configurations the interaction energies at the different levels of theory considered, with and without BSSE correction, as well as the first harmonics, are reported in Table 6. Interaction energies and associated wavenumbers were obtained using  $\omega$ B97X-D and 6-311G, 6-311G\*\* and cc-pVDZ basis sets. Computed values are compared with results obtained by Walsh et al [54], Saeki et al [1] and Rubes et al [55]. BSSE-correction lowers the absolute value of the energy by 1.5 kcal.mol<sup>-1</sup> on average, and represents only 0.04% of the binding energy. Thus BSSE-correction does not affect the order of stability of the tested configurations. This

## III.2. Calculation of vibrational spectra of acene dimers: Comparison with experimental data.

outcome is in full agreement with the cited prior work. Further there are no trends for the impact of basis-set and BSSE-correction on the geometry of the dimer configurations. However, by calculating the mean difference of computed values, this work, with those of Saeki et al [1] shows the 6-311G basis-set combined with BSSE-correction to be a preferred option.

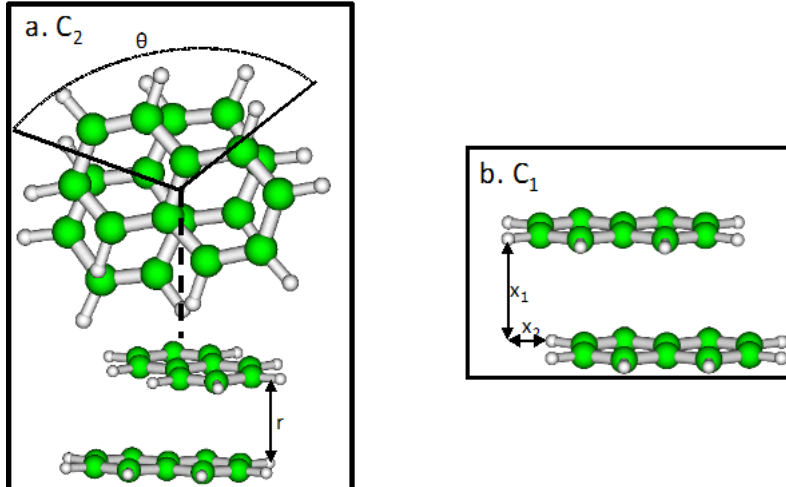


Figure 1.5 – Optimized geometries at the  $\omega$ B97X-D/6-311G level of theory for naphthalene dimers in the most stable configurations a)  $C_2$ , and b) Parallel-displaced (PD)

Table 1.5 – Geometry dependence of basis sets on structures PD and  $C_2$  shown in Figure 4.5

	$C_2$	PD			
	$\Theta(^{\circ})$	$r(\text{\AA})$	$r(\text{\AA})$	$x_1(\text{\AA})$	$x_2(\text{\AA})$
6-311G	129	3.38	3.52	1.12	1.26
+CP <sup>a</sup>	126	3.41	3.44	1.08	1.29
6-311G**	130	3.45	3.32	1.07	1.27
+CP <sup>a</sup>	133	3.43	3.65	1.05	1.30
cc-pVDZ+CP <sup>a</sup>	134	3.45	3.49	1.11	1.28
Saeki et al[1]	135	3.46	3.40	1.03	1.31

<sup>a</sup> CP refers to the keyword “counterpoise” used in Gaussian to take BSSE-correction in account in the calculations.

Table 1.6 – Interaction energies in kcal/mol and associated wavenumber ( $\text{cm}^{-1}$ ) of optimized naphthalene dimers.

Naphthalene		$\mathbf{C}_2$		PD
$\omega\text{B97X-D}/\text{6-311G}$ (This work)	without counterpoise	-9.00	14	-8.72
	with counterpoise	-7.55	8	-7.28
$\omega\text{B97X-D}/\text{6-311G}^{**}$ (This work)	without counterpoise	-9.45	16	-9.16
	with counterpoise	-7.86	12	-7.58
$\omega\text{B97X-D/cc-pVDZ}$ (This work)	with counterpoise	-7.52	12	-7.22
$\text{MP2}/\text{6-31G}^*$ (0.25) (Walsh et al[54])	with counterpoise	-8.15		-7.68
$\text{MP2}/\text{cc-pVDZ}$ (Saeki et al[1])	without counterpoise	-5.30	22	-5.00
	with counterpoise	-6.24		-5.89
$\text{DFT/CCSD(T)}$ (Rubes et al[55])		-6.23		-5.96
$\text{SAPT0/aug-cc-pVDZ}$ (Hohenstein et al[57])				-7.27

**Vibration modes of naphthalene dimers:** Wavenumber calculations for stable dimers were performed using the  $\omega\text{B97X-D}/\text{6-311G}$  method with BSSE correction. From vibrational analysis of the monomer (Table A2 in the supplementary data) and the dimer (Table 1.7) the vibrational modes arising from intra- and intermolecular modes can be discriminated. The assignments are reported in Table 1.7 for sets of calculations performed as part of this work and from Saeki et al[1]. Calculated values are compared with experimental data when available. The calculations were performed with counterpoise correction for both the  $\mathbf{C}_2$  and PD configurations. The calculated intra- and intermolecular wavenumbers, irrespective of calculation details, are readily distinguished for naphthalene. The intermolecular wavenumbers are at  $\sim 100 \text{ cm}^{-1}$  and lower, while the intramolecular wavenumbers are greater than  $\sim 100 \text{ cm}^{-1}$ .

Table 1.7 – Calculated wavenumber ( $\text{cm}^{-1}$ ) of the intra- and intermolecular vibrational modes of the naphthalene dimer in the configuration a) and b) at the  $\omega\text{B97X-D}/6-311\text{G}$  level with BSSE-correction, compared with frequencies obtained at the MP2/cc-pVDZ level in the article of Saeki et al[1].

Configuration C <sub>2</sub> $\omega\text{B97X-D}/6-311\text{G}^a$		Saeki et al[1] MP2/cc-pVDZ <sup>b</sup>		Configuration PD $\omega\text{B97X-D}/6-311\text{G}^a$		Saeki et al[1] MP2/cc-pVDZ <sup>b</sup>	Experimental values[58]
Harmonic	PT2	Harmonic	PT2	Harmonic	PT2		
<b>Intramolecular</b>							
184	181	185	188	181	180	176	
192	187	188	196	188	187	195	
199	198	203	207	201	201		
203	202	205	208	201	207		
378	370	351	380	372	351		
378	371	351	381	372	351	359	
404	398	386	405	396	385		
405	398	387	405	397	387		
<b>Intermolecular</b>							
14	16	22	33	29	8		
32	34	45	36	35	39		
50	50	64	55	51	54		
78	83	95	75	68	81		
85	89	103	88	85	100		
94	99	106	101	98	110		

<sup>a</sup> with counterpoise correction

<sup>b</sup> without counterpoise correction

### 1.2.2 $\pi$ -stacking in the acene family

Optimization at the  $\omega\text{B97XD}/6-311\text{G}$  level with BSSE correction gives rise to the expected parallel tilted configuration [51] for anthracene, tetracene and pentacene dimers, as shown in Figure 6. This configuration closely resembles that found in triclinic tetracene[4] and pentacene[7] crystals. The associated interaction energies are reported Table 1.8. Other configurations were found to be unstable. They possess negative calculated harmonic values and were clearly not located at a minimum of the PES. So, only naphthalene has a more energetically stable C<sub>2</sub> configuration. Computations related to both the C<sub>2</sub> and PD configurations for naphthalene are shown in Table 1.7. The PD configuration results are used for comparisons with other acene family members where it is the most stable configuration. For a given geometry, in this case parallel-tilted, the binding interaction energy increases with the number of interacting cycles in a non-linear manner. This result is consistent with previous studies by Hohenstein et al [57] and Grimme et al[59] who compared interaction energies of naphthenic and aromatic dimers of increasing size using the B2PLYP/TZV(2d,p) level of theory. They found that arene dimers were strongly preferred over equivalent naphthenic dimers, especially for anthracene and tetracene, which were stabilized by 3 to 4 kcal. $\cdot\text{mol}^{-1}$ . The calculations reported here are in accordance with these prior results and confirm the prevalence of  $\pi$ -stacking interactions.

The wavenumbers assigned to intermolecular (Table 1.9) and intramolecular (Table 1.10) modes of vibration for the acene family were calculated at the  $\omega\text{B97XD}/6-311\text{G}$  level of theory using BSSE correction. The characteristic wavenumbers for intermolecular vibrations fall in the same range for all acene dimers. The lower bound wavenumbers are 15 - 33  $\text{cm}^{-1}$  and the upper bound wavenumbers are 94 - 112  $\text{cm}^{-1}$ . The wavenumbers for the intramolecular vibrations are found at higher wavenumbers but begin to overlap with the intermolecular vibration

wavenumbers starting with anthracene where the intermolecular mode at a wavenumber of  $111\text{ cm}^{-1}$  with an intensity of 0.8 is not readily discriminated from the intramolecular mode at  $112\text{ cm}^{-1}$  with an intensity of 1.2, on the basis of wavenumber or intensity value. Thus, inter and intramolecular vibrations are easily discriminated for naphthalene, and the inter- and intramolecular vibration modes are uncorrelated. For anthracene, tetracene and pentacene, the lowest intramolecular vibration modes fall within the range of intermolecular vibrations.

Four vibration modes, given in Table 1.9, corresponding to rotation, translation, rotation of the dimer combined with translation and rotation movements of one molecule relative to the other, are common for all four dimers. The last two intermolecular modes are compound-specific. For tetracene, the two additional modes comprise twisting movements of molecular pairs in the same ( $87\text{ cm}^{-1}$ ) and in the opposite direction ( $112\text{ cm}^{-1}$ ). For pentacene, one is a wagging movement ( $74\text{ cm}^{-1}$ ) and the other comprises an opposite direction wagging movement combined with vertical translation normal to the two molecules ( $95\text{ cm}^{-1}$ ). For anthracene, one mode is a rotation of one molecule relative to the other, and the second is split into two modes. These latter two modes, at  $111$  and  $112\text{ cm}^{-1}$ , consist of a butterfly movement by one molecule with a half-twisting movement by the other simultaneously.

The other vibration modes, shown in Table 1.10 correspond to intramolecular vibrations. For every type of vibration, simultaneous vibration of each molecule is observed, either in the same or opposite direction, resulting in two wavenumbers. These alternating motions are characterized by wavenumbers and intensities that depend on the value of the dipole moment. The butterfly vibration mode presents very different wavenumbers depending on whether the molecular movements are in the same or opposite direction. Differences range in value from 8 to  $42\text{ cm}^{-1}$ . The impact of relative movement increases with the number of aromatic rings, due to the correlation with twisting modes at higher frequencies.

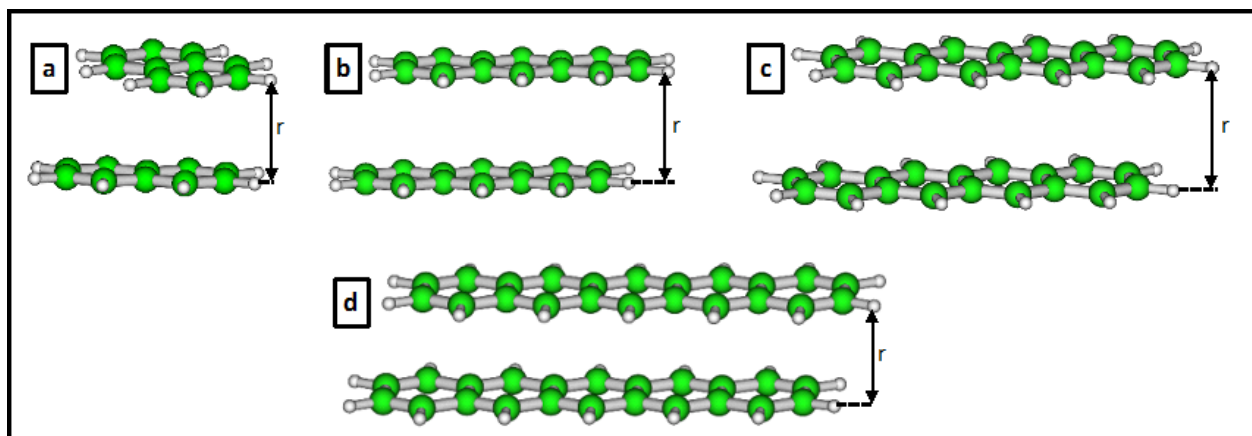


Figure 1.6 – Acene dimers in the parallel displaced (PD) configuration: a) naphthalene, b) anthracene, c) tetracene, d) pentacene

## 21.2. Calculation of vibrational spectra of acene dimers: Comparison with experimental data.

Table 1.8 – Intermolecular distance and Interaction energies calculated for acene dimers.

Dimers		Naphthalene	Anthracene	Tetracene	Pentacene
Intermolecular distance r(Å)		3.41	3.27	2.96	2.98
Interaction energies kcal/mol	$\omega$ B97XD/6-311G + BSSE corection Hohenstein et al[57]	-7.53	-11.52	-15.73	-20.44
	SAPT0/aug-cc-pVDZ	-7.27	-12.24	-17.49	-22.91

Table 1.9 – Calculated intermolecular vibrational modes ( $\text{cm}^{-1}$ ) and their intensities for naphthalene, anthracene, tetracene and pentacene dimers.

Type*	naphthalene	anthracene	tetracene	pentacene
Rotation 1/2	33(0.04)	22(0.004)	15(0.002)	19(0.002)
Translation 1/2	36(0)	34(0)	31(0)	27(0)
Total rotation + Translation 1/2	55(0)	57(0)	52(0)	57(0)
	75(0.21)	75(0.05)	87(0.14)	74(0.07)
Rotation 1/2	88(0.08)	87(0.8)	80(0.96)	72(0.9)
	101(0)	111(0.8)/112(1.2)	112(0)	95(0)

\* 1/2 means one molecule relative to the other one

**Trends in values for specific bands in the acene family:** In order to visualize the effect of the number of aromatic rings on the wavenumbers of specific vibration modes, intramolecular vibration modes and intermolecular vibrations are presented in Figure 1.7 and Figure 1.8, respectively. Intramolecular vibration modes, shift to lower wavenumbers with increasing molecule size irrespective of the vibrational mode considered, as was observed for monomers. Butterfly (B), Twisting ( $\tau$ ), Wagging ( $\omega$ ), Stretching ( $\sigma$ ), and Rocking ( $\rho$ ) movements behave similarly. By contrast, the intermolecular vibration modes, found at similar wavenumbers for all the molecules in the acene family, appear specific to this family, and may be used as a reliable fingerprint. In addition, twisting vibration bands appear for dimers of tetracene at ( $208 \text{ cm}^{-1}$ ) and pentacene at ( $168 \text{ cm}^{-1}$ ) that replace corresponding twisting bands for monomers at  $154$  and  $104 \text{ cm}^{-1}$ . The absence of a mode at  $154 \text{ cm}^{-1}$  for tetracene dimers supports the hypothesis that the feature observed experimentally at  $142 \text{ cm}^{-1}$  for monomers (see Table 1.3) is an overtone.

### 1.2.3 The impact of molecule distortion on the vibration modes of acene dimers

The impact of molecular distortion on vibration modes for dimers was evaluated in the same manner as for monomers. The molecular conformations were perturbed as illustrated in Figure 3 and the distance  $r$  (defined in Figure 1.6) between the molecules was set equal to 3.4, 3.4 and

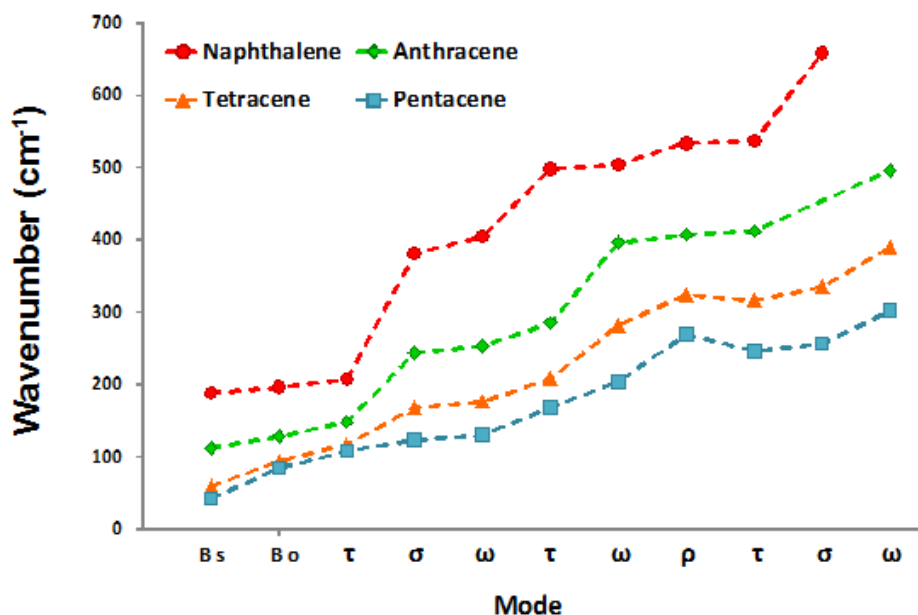


Figure 1.7 – Comparison of theoretical intramolecular vibration modes for naphtalene, anthracene, tetracene and pentacene dimers: B s and B o designate butterfly modes, same (s) and opposite (o) direction respectively;  $\tau$ ,  $\sigma$ ,  $\omega$ , and  $\rho$  take place for twisting, stretching, wagging and rocking modes respectively

2.9 Å for naphthalene, anthracene and tetracene dimers, respectively. As distortion reduces the aromaticity of the molecules, the stability of  $\pi$ -stacked dimers is expected to be reduced or eliminated. Table 11, where interaction energies for these systems are listed, highlights this loss of stability. For example, no conformations for distorted pentacene dimers correspond to local minima in the PES. Distortion did not affect intramolecular modes of vibration overall for dimers as shown in Table A3 in the supplementary data. Only butterfly vibration modes for anthracene and tetracene, whose wavenumbers get closer to the ones observed for monomers, shown in Table 1.10, appear to be affected. Some other modes, for which two wavenumbers are given in Table A3, do not exhibit the combined movement of the two molecules either in the same direction or in the opposite direction (as observed for the other intramolecular modes), but movement of the molecules simultaneously. These exceptions are a consequence of the decoupling between the molecules forming the distorted dimer. However, the intermolecular vibration modes, shown in Table 1.12, are shifted to lower wavenumbers compared to the symmetric analogues shown in Table 1.9. For the symmetric dimers, the intermolecular vibration modes are effectively independent of molecule size, while for the distorted molecules, the vibration modes tend to lower values as molecular size increases. The behavior of the symmetric dimers is attributed to a balancing of opposing effects. One would expect intermolecular vibration modes to shift to lower wavenumbers with increasing ring number (as is observed for intramolecular modes). However, the intensity of the intermolecular interactions increases with the number of rings (Table 1.8) for symmetric dimers, and this tends to increase wavenumbers. This compensative effect is diminished or absent for the distorted dimers, hence the difference in behavior, and wavenumber invariance for a given intermolecular vibration mode may be a characteristic of  $\pi$ -stacking interactions.

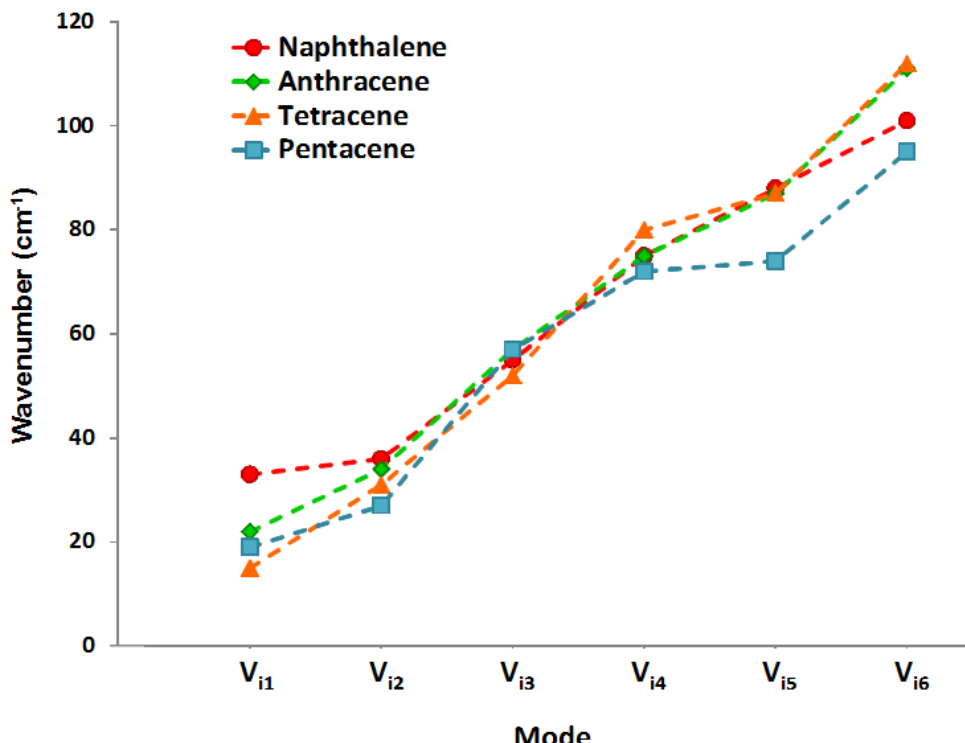


Figure 1.8 – Comparison of theoretical intermolecular vibration modes for naphthalene, anthracene, tetracene and pentacene dimers

#### 1.2.4 Identification of unassigned peaks in the experimental spectra of tetracene and pentacene

By subtracting the intermolecular wavenumbers from the symmetric dimer vibrational spectra of tetracene and pentacene, and comparing the resultant spectra with the spectra of the corresponding monomers, there are two peaks, one for tetracene at  $117\text{ cm}^{-1}$  and one for pentacene at  $108\text{ cm}^{-1}$ , with intensities in the same order of magnitude as the ones calculated for fundamental bands for tetracene ( $0.34\text{ km/mol}$ ) and pentacene ( $0.15\text{ km/mol}$ ). These peaks arise because for every vibrational mode occurring for monomers, there are two quasi-degenerate modes arising for dimers depending on whether the molecules vibrate in the same or in the opposite direction. Thus modes that are Raman-active for a monomer become infrared-active for dimers vibrating in the opposite direction.

With this final set of assignments, the inter- and intramolecular vibration analysis for the acene family of compounds is complete. Figure 1.9 gives a direct comparison of experimental and calculated spectra with our conclusion as for assignment. There are no residual unassigned peaks in the available experimental spectra and ultra low wavenumber intermolecular peaks are hypothesized. While these have yet to be measured experimentally, identification and discrimination of inter- and intramolecular bands at low wavenumbers will play a more important role in the future as the range of IR measurements broadens. For example, by using coherent synchrotron radiation it is becoming possible to make experimental photoacoustic IR measurements in the range  $7$  to  $30\text{ cm}^{-1}$  as demonstrated recently by Billinghamurst and Michaelian[60]. DFT calculations have much to contribute to this development, and the interpretation of results obtained.

Table 1.10 – Intramolecular vibration modes ( $\text{cm}^{-1}$ ) and the corresponding intensities in brackets (km/mol) for naphthalene, anthracene, tetracene and pentacene dimers. Values of corresponding monomer modes are written below in italics.

Type*	naphthalene	anthracene	tetracene	pentacene
Butterfly sw	188(3.8)	111(0.8)/112(1.2)	59(0.6)	42(0.4)
	<i>177(3.2)</i>	<i>93(1.5)</i>	<i>57(0.8)</i>	<i>38(0.5)</i>
Butterfly ow	196(0)	128(0)	94(0)	84(0)
	<i>177(3.2)</i>	<i>93(1.5)</i>	<i>57(0.8)</i>	<i>38(0.5)</i>
Twisting sw	207(1.2)	148(0.6)	117(0.3)	108(0.2)
	<i>191(0)</i>	<i>124(0)</i>	<i>93(0)</i>	<i>74(0)</i>
Twisting ow	208(0)	149(0.02)	124(0)	101(0.002)
	<i>191(0)</i>	<i>124(0)</i>	<i>93(0)</i>	<i>74(0)</i>
Scissoring sw	381(2.2)	244(2.1)	168(1.7)	123(1.5)
	<i>379(1.5)</i>	<i>243(1.4)</i>	<i>168(1.3)</i>	<i>123(1.0)</i>
Scissoring ow	380(0)	243(0)	169(0)	125(0)
	<i>379(1.5)</i>	<i>243(1.4)</i>	<i>168(1.3)</i>	<i>123(1.0)</i>
Wagging sw	405(0)	250(0)	162(0)	116(0)
	<i>403(0)</i>	<i>276(1.1)</i>	<i>196(0)</i>	<i>150(0)</i>
Wagging ow	405(0.02)	253(0.2)	176(0.2)	130(0.08)
	<i>403(0)</i>	<i>276(1.1)</i>	<i>196(0)</i>	<i>150(0)</i>
Twisting sw	498(0)	285(0.02)	208(0)	168(0.05)
	<i>494(0)</i>	<i>281(0)</i>		
Twisting ow	499(15.2)	286(0.08)	212(0.09)	168(0.2)
	<i>494(0)</i>	<i>281(0)</i>		
Wagging sw	504(45.0)	396(0.2)	282(1.6)	204(2.2)
	<i>504(28.7)</i>	<i>394(0.05)</i>	<i>276(1.1)</i>	<i>198(1.3)</i>
Wagging ow	507(0)	396(0.04)	286(0)	210(0.002)
	<i>504(28.7)</i>	<i>394(0.05)</i>	<i>276(1.1)</i>	<i>198(1.3)</i>
Stretching sw	534(0)	407(0)	324(0)	269(0)
	<i>534(0)</i>	<i>407(0)</i>	<i>324(0)</i>	<i>269(0)</i>
Stretching ow	534(0.09)	407(0.04)	325(0.06)	269(0.05)
	<i>534(0)</i>	<i>407(0)</i>	<i>324(0)</i>	<i>269(0)</i>
Rocking sw	537(0)	412(0)	316(0)	246(0)
	<i>537(0)</i>	<i>412(0)</i>	<i>316(0)</i>	<i>247(0)</i>
Rocking ow	537(0.06)	412(0.01)	316(0.03)	247(0.05)
	<i>537(0)</i>	<i>412(0)</i>	<i>316(0)</i>	<i>247(0)</i>
Twisting sw	658(0.4)		335(0.03)	256(0.02)
	<i>656(0)</i>		<i>327(0)</i>	<i>247(0)</i>
Twisting ow	659(0)		336(0)	257(0.008)
	<i>656(0)</i>		<i>327(0)</i>	<i>247(0)</i>
Wagging sw		496(70.5)	390(0)	302(0.005)
		<i>495(0)</i>	<i>389(0)</i>	<i>247(0)</i>
Wagging ow		496(0.5)	390(0.02)	303(0.07)
		<i>495(0)</i>	<i>389(0)</i>	<i>247(0)</i>

\*sw same way (i.e. resulting dipole moment in the same direction for the two molecules)

\*ow opposite way (i.e. resulting dipole moment in opposite direction for the molecules)

Table 1.11 – Interaction energies calculated for distorted acene dimers.

Dimers	naphthalene	anthracene	tetracene	
Interaction energies (kcal/mol)	$\omega$ B97XD/6-311G + BSSE correction	+1.23 (+8.76)	-4.27 (+7.25)	-10.81 (+4.92)

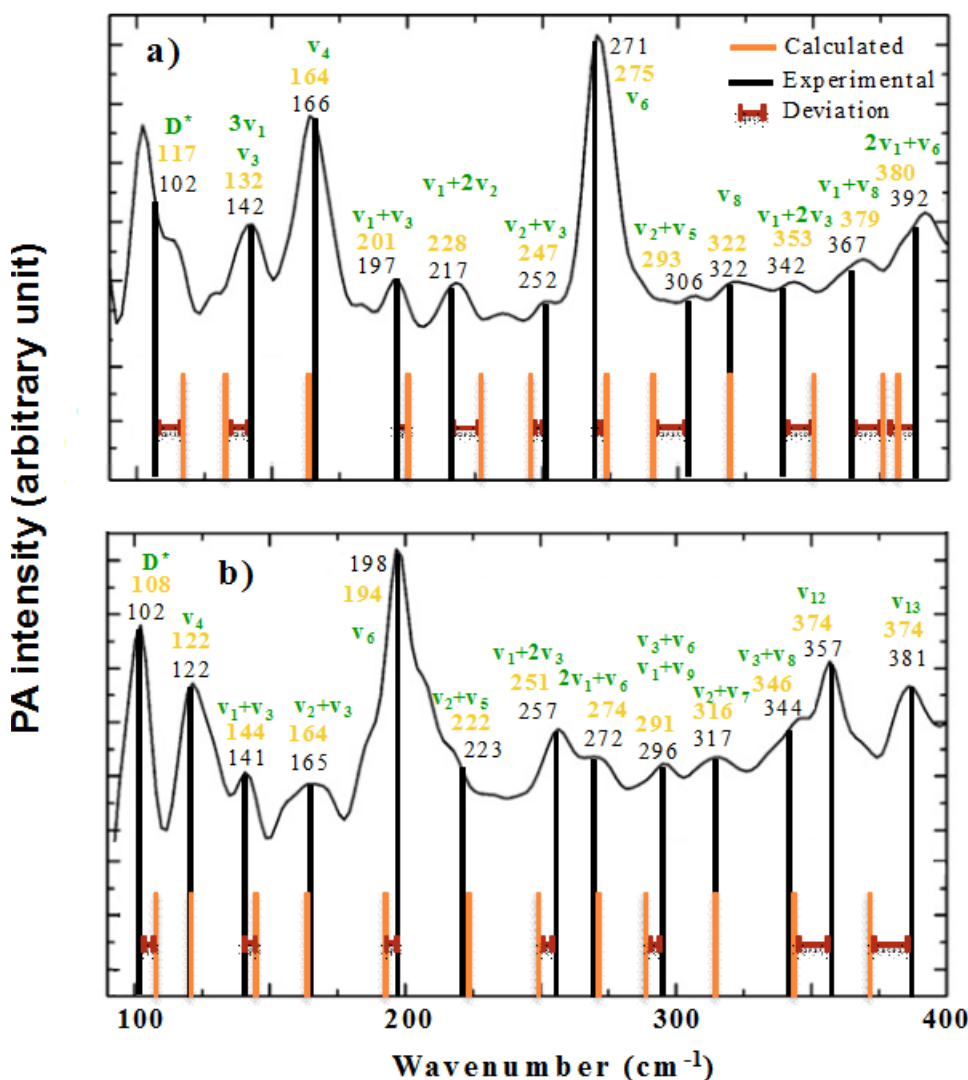


Figure 1.9 – Final assignment of the experimental infrared transitions for a) tetracene and b) pentacene. Calculated wavenumbers are indicated on the spectra with orange lines, and corresponding values above. Experimental values are indicated for comparison, and represented with dark lines

Table 1.12 – Calculated intermolecular vibrational modes ( $\text{cm}^{-1}$ ) and their intensities for distorted dimers of naphthalene, anthracene and tetracene.

Type*	naphthalene	anthracene	tetracene
Translation 1/2	12(0.015)	11(0.004)	6(0)
Rotation 1/2	32(0.04)	21(0.004)	13(0.004)
Translation 1/2	47(0.007)	33(0.002)	21(0.005)
Rotation + Translation	60(0.006)	41(0.009)	33(0.003)
Translation (remoteness of molecules)	73(0.008)	55(0.01)	46(0.2)
Rotation 1/2	94(0.14)	73(0.2)	
Twisting of the full system			74(0.08)

\* 1/2 means one molecule relative to the other.

### 1.3 Normal Vibrational Modes in Crystals

We performed first-principle calculations for tetracene in order to clarify its structural and electronic properties of the solid-state system. These calculations strongly suggest the necessity to go beyond the standard DFT approach. First, we have shown that dispersion corrected methods are necessary to provide an improvement in the calculated lattice parameters and volume of the unit cell to compare with experimental values. The complete list of resulting lattice parameters, angles, and volumes along with experimental results for all the compounds are presented in Table 1.13. Furthermore, the mean absolute deviations observed for the calculation of these parameters for all the methods under consideration depend on the type of dispersion correction, and the relative errors on structural properties calculated using each method, in particular concerning the volume, may vary significantly. As mentioned by Lebegue et al [61], it has been demonstrated that one has to test all the dispersion corrected DFT methods for the C-, H-, N- and O- based energetic solids before concluding the ground state properties. In the present work, we show that the situation is the same for the S-based energetic solids. Since the D3 correction yields the most accurate structural descriptions of this model system, it has been used to calculate the vibrational, structural and electronic properties.

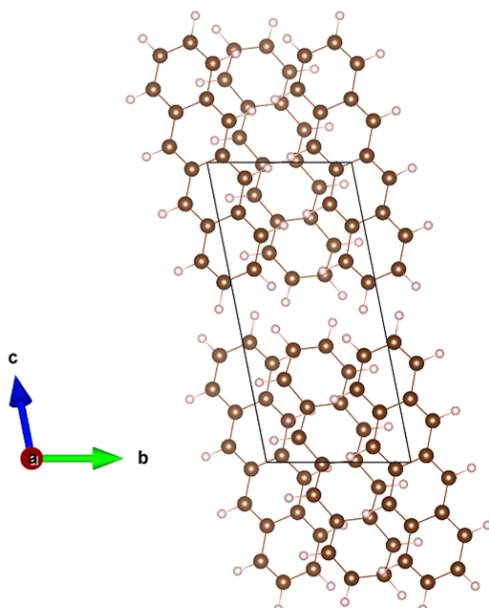
Table 1.14 reports all the results obtained for tetracene, from the isolated up to the solid-state system. Beyond the numerical differences due to the various Hamiltonians used for these calculations, the results show significant differences on both vibration frequencies and intensities that are to be attributed to the effect of the chemical environment. Indeed, the signatures of some particular modes (such as  $\nu_2$ ,  $\nu_8$  and  $\nu_{10}$ ) are modified with respect to the isolated system due to intermolecular interactions. Besides, our previous study on tetracene dimers revealed that intermolecular interactions induced the appearance of some characteristic spectral signatures at very low wavenumbers. For instance, the mode experimentally found at  $106 \text{ cm}^{-1}$ , which has been assigned, with aid of calculations, to a libration mode, is part of the characteristic signatures of intermolecular vibrations of acenes; the same mode was also assigned

Table 1.13 – Lattice parameters of Tetracene molecule calculated in VASP code

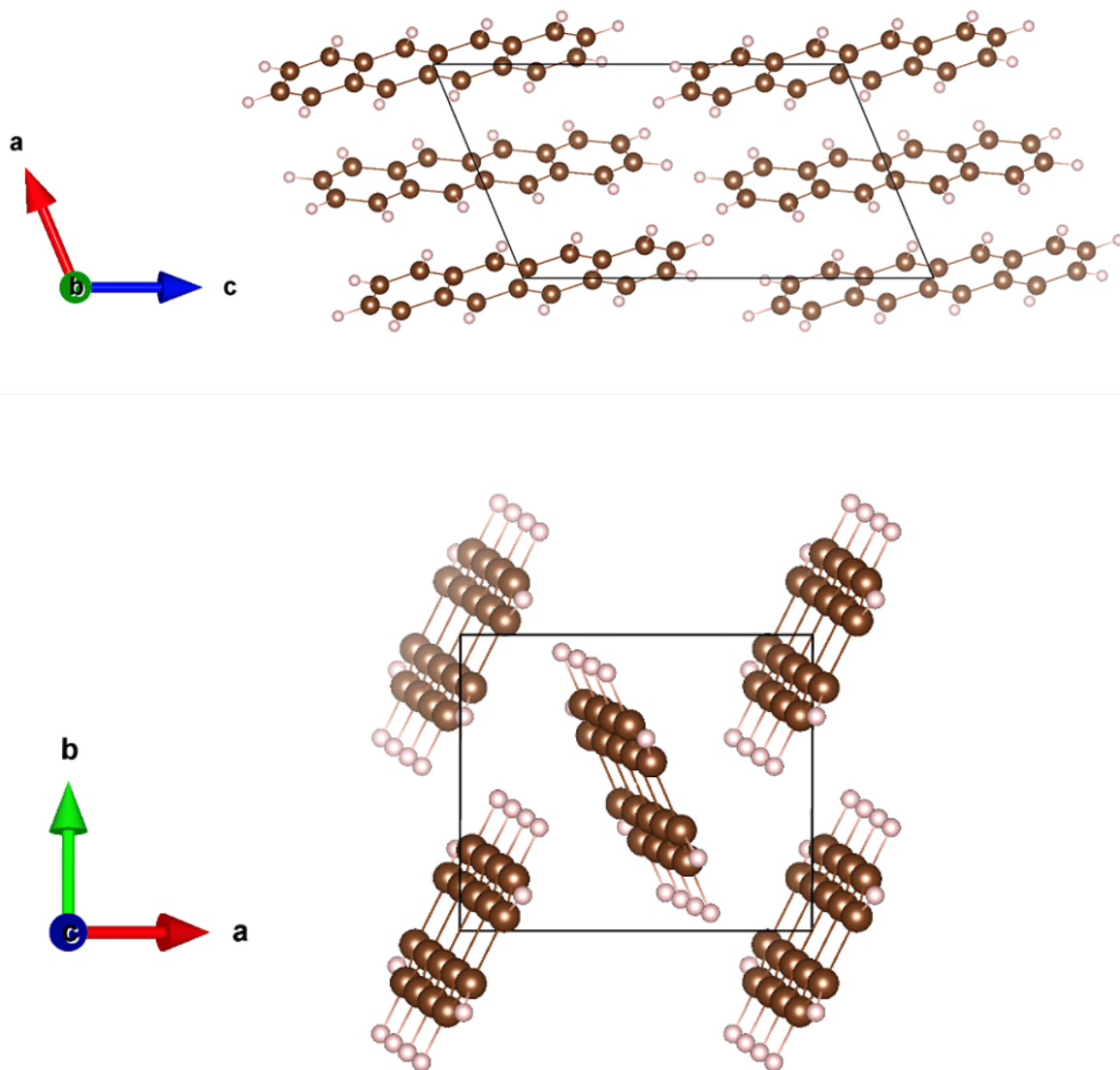
	D2	D3	TS	TS-SCS	PBE*	Exp
<b>a</b>	7.54 (7.41)	7.92	7.71	7.70	9.25	7.90
<b>b</b>	5.96 (5.83)	6.00	5.99	6.08	7.21	6.03
<b>c</b>	13.28 (13.39)	13.38	13.38	13.47	16.62	13.53
$\alpha$	102.10 (102.21)	101.21	101.36	100.97	101.36	100.30
$\beta$	114.33 (113.23)	113.26	113.61	114.39	112.14	113.20
$\gamma$	85.20 (85.11)	85.89	85.74	85.68	86.67	86.30
<b>Volume (Å<sup>3</sup>)</b>	531.41 (519.01)	572.96	554.74	563.74	1007.16	582.85

\* without dispersion correction

(<sup>o</sup>) Parenthesis values were calculated with CRYSTAL program



at  $102\text{ cm}^{-1}$  for the pentacene system. In fact, this mode cannot be only associated to a dimer: it results from the vibrations of the whole tetracene molecules within the network that constitutes the aggregate or the crystalline system. Our VASP calculations clearly show that this vibration mode is linked to distortions of the crystalline network, which can be seen as the « breathing » of the network. Such a deformation was already partially taken into account in the study of a dimer. Some other modes of the crystalline network constitute, to a lesser extent, the remaining characteristic signatures of the intermolecular vibrations. More difficult to detect experimentally, these modes are theoretically found at  $69.7\text{ cm}^{-1}$  ( $\nu_1$ ),  $128.5\text{ cm}^{-1}$  ( $\nu_3$ ) and  $320.8\text{--}323.8\text{ cm}^{-1}$  ( $\nu_8$ ). Unfortunately, there is no experimental data available below  $100\text{ cm}^{-1}$  for the tetracene system. But it seems that the  $\nu_3$  and  $\nu_8$  modes can now be identified as the modes of medium intensity reported from experimental data at  $142$  and  $322\text{ cm}^{-1}$ , respectively. No fundamental mode nor combination mode of the isolated tetracene can be associated with the presence of those new experimental signatures.



From all the modes calculated below  $400 \text{ cm}^{-1}$ , whatever their intensities are, they do not seem to be coupled to the vibration of the crystalline network. It suggests that calculations of the isolated molecule (or its dimer) are a sufficient approximation to identify these vibration modes. In the present case, it explains the fact that no assignation problem was found for regions beyond  $150 \text{ cm}^{-1}$  during the molecular study of tetracene and its dimer. At the molecular level, calculations on small aggregates can be sufficient to identify the modes of the crystalline network that are significantly impacted.

To conclude, the use of a model able to describe the chemical environment was essential to identify the spectral signatures of the inter-molecular modes that we try to characterize in our study of asphaltenes (or, at least, of acenes systems). The calculated phonon spectrum thus seems to answers, even if our calculations up to now do not account for both mechanical and electrical anharmonicities. Such conditions are all the more necessary for an exhaustive study of the modes of each isolated molecule. Particularly, it allows an identification of the combination modes as well as the harmonics for which the signatures have been clearly evidenced by photo-acoustic measurements. Only a double approach (both molecular and solid-state) can allow one to completely identify the photo-acoustic results of acenes molecules in the crystalline state.

Table 1.14 – Calculated vibrational frequencies ( $\text{cm}^{-1}$ ) of the monomer, dimer and solid-state (PBE tetracene system).

	<b>Monomer</b>	<b>Dimer</b>	<b>Experimental (P.A.) this work</b>	<b>VASP/CRYSTAL</b>
Assignment	$\nu(\text{cm}^{-1})$ Int(km/mol)	$\nu(\text{cm}^{-1})$ Int(km/mol)	$\nu(\text{cm}^{-1})$	$\omega(\text{cm}^{-1})$ Int(relative)
$\nu_1$	57 (0.8)	15 (<0.01) 31 (0) 52 (0)	69.7 (8.2)	
$\nu_2$	93 (0)	59 (0.6) 80 (1.0) 87 (0.1) 94 (0) 112 (0) 124 (0)	106 (m) + sh	102.4 (2.1) 105.7 (9.5)
$3\nu_1$	132 (<0.01)			
$\nu_3$	153 (0.01)		142 (m)	128.5 (7.1) 148 (0.1)
$\nu_4$	164 (1.3)	162 (0) 168 (1.7) 169 (0)	166 (s) + sh	164.6 (15.5)
$\nu_5$	199 (0.05)	176 (0.2)	197 (w)	170.1 (0.1)
$\nu_1 + \nu_3$	201 (<0.01)	208 (0) 212 (0.09)	217 (w)	
$\nu_1 + 2\nu_2$	228 (<0.01)			
$\nu_2 + \nu_3$	247 (0.01)		252 (vw)	
$\nu_6$	275 (1.03)	282 (1.6) 286 (0)	271 (m)	267.4 (3.0) 274.6 (2.6)
$\nu_2 + \nu_5$	293 (<0.01)		306 (vw)	
		316 (0)		
		316 (0.03)		
		324 (0)	322 (w)	320.8 (0.9)
$\nu_8$	322 (<0.01)	325 (0.06) 335 (0.03) 335 (0)	342 (w)	323.8 (0.5)
$\nu_1 + 2\nu_3$	353 (<0.01)			
$\nu_1 + \nu_8$	379 (<0.01)			
$\nu_{10}$	385 (0.04)	390 (0.02)	392 (m)	
$2\nu_1 + \nu_6$	380 (<0.01)			

Italic: Intermolecular modes

We are aware that it is not possible to jump to conclusions on the basis of the results of a single system. In the same way, additional calculations were performed within this work for other compounds of the acene family, as well as other systems of the aromatic polycycle molecules family. The aim of these additional calculations is verifying if the position and activity of the network modes identified for the tetracene molecule, and particularly the mode clearly localise at around  $106\text{ cm}^{-1}$ , depend on the size, length or on the moiety of the polycycle system in study.

The first parameter we studied is the chain-length within the acene family. A series of calculations on the benzene, naphthalene, anthracene and pentacene calculations was performed. The crystalline structures from which we were able to do our calculation are presented hereafter. More particularly, the benzene molecule has three different phases: Phase I correspond to an orthorhombic Pbca space group that contain four molecules per unit cell. In opposite, the two other phases called II and III contain two molecules in the unit cell and crystallizes in a monoclinic system (space group P21/c) at high pressure [62, 63]. In that case molecule configuration observed by differents study is T-Shape [63]. Under ambient conditions of temperature and under low-pressure, crystals of the naphthalene belong to the monoclinic system (space group P21/a) and contain two molecules per unit cell [64]. Under the same conditions, the crystals of both anthracene and tetracene crystallize in a monoclinic phase P21/a [51] and in a triclinic phase P1̄ [65] respectively. Crystals of the pentacene system crystallize into a triclinic phase (space group P1̄); it is reported to have two polymorphs structures in its bulk phase, polymorph C [4] and polymorph H [6]. The ensemble of the numerical results relative to the cell parameters and cell volumes can be found in Tables 1.15, 1.16, 1.17, 1.18 and 1.19 . A representation of these crystalline cells is given in Figures 1.10, 1.11, 1.12 and 1.13.

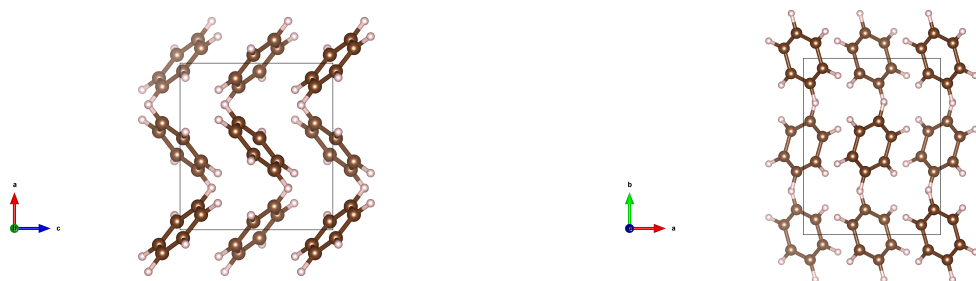


Figure 1.10 – The *ac* and *ab* planes of benzene crystal

Table 1.15 – Lattice parameters of benzene molecule calculated in VASP code

	D2	D3	TS	TS-SCS	PBE*	Exp
<b>a</b>	7.24 (6.90)	7.45	7.32	7.33	8.29	7.36
<b>b</b>	9.09 (9.13)	9.54	9.41	9.42	10.35	9.37
<b>c</b>	6.63 (6.55)	6.84	6.71	6.72	7.73	6.70
<b>Volume (Å³)</b>	434.57 (412.45)	485.94	462.14	463.15	662.85	465.60

\* without dispersion correction

① Parenthesis values were calculated with CRYSTAL program

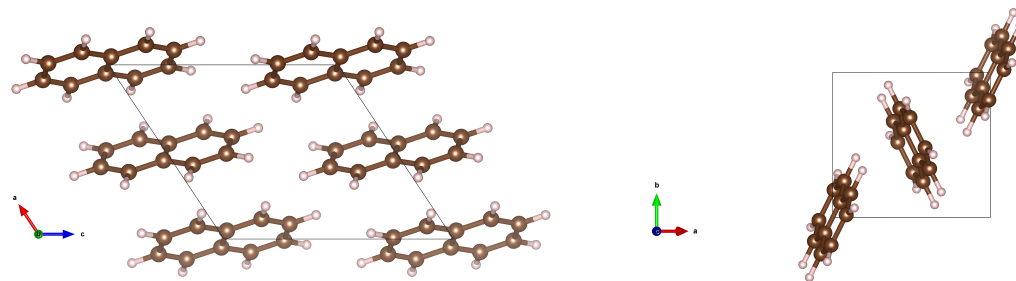
Figure 1.11 – The *ac* and *ab* planes of Naphthalene crystal

Table 1.16 – Lattice parameters of naphthalene molecule calculated in VASP code

	D2	D3	TS	TS-SCS	PBE*	Exp
<b>a</b>	7.71 (7.78)	8.00	7.85	7.89	9.64	8.03
<b>b</b>	5.84 (5.74)	6.07	6.01	6.03	6.51	5.89
<b>c</b>	8.50 (8.57)	8.68	8.63	8.65	9.14	8.57
$\beta$	125.18 (125.25)	123.40	123.68	123.69	121.46	123.59
<b>Volume (Å³)</b>	313.24 (312.75)	351.97	338.45	342.52	488.96	337.65

\* without dispersion correction

① Parenthesis values were calculated with CRYSTAL program

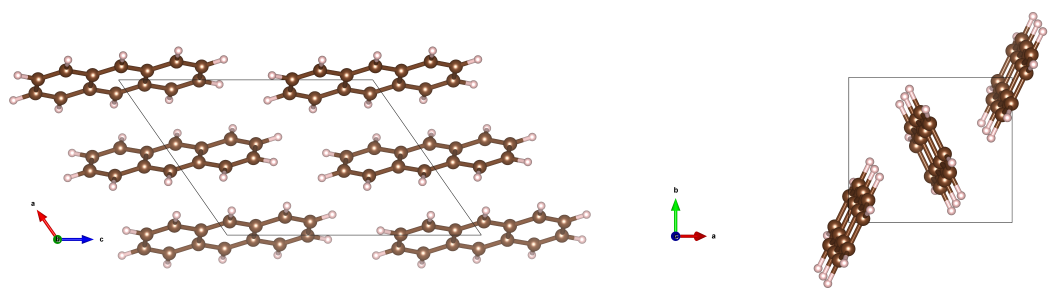
Figure 1.12 – The *qc* and *ab* planes of anthracene crystal

Table 1.17 – Lattice parameters of anthracene molecule calculated in VASP code

	D2	D3	TS	TS-SCS	PBE*	Exp
<b>a</b>	8.04 (8.40)	8.39	8.23	8.26	9.97	8.55
<b>b</b>	5.99 (5.67)	6.12	6.03	6.07	6.54	6.02
<b>c</b>	11.14 (11.30)	11.25	11.17	11.21	11.60	11.17
$\beta$	126.09 (128.26)	124.95	125.46	125.42	121.61	124.60
<b>Volume (Å<sup>3</sup>)</b>	433.85 (422.71)	473.17	452.06	457.75	644.25	473.17

\* without dispersion correction

() Parenthesis values were calculated with CRYSTAL program

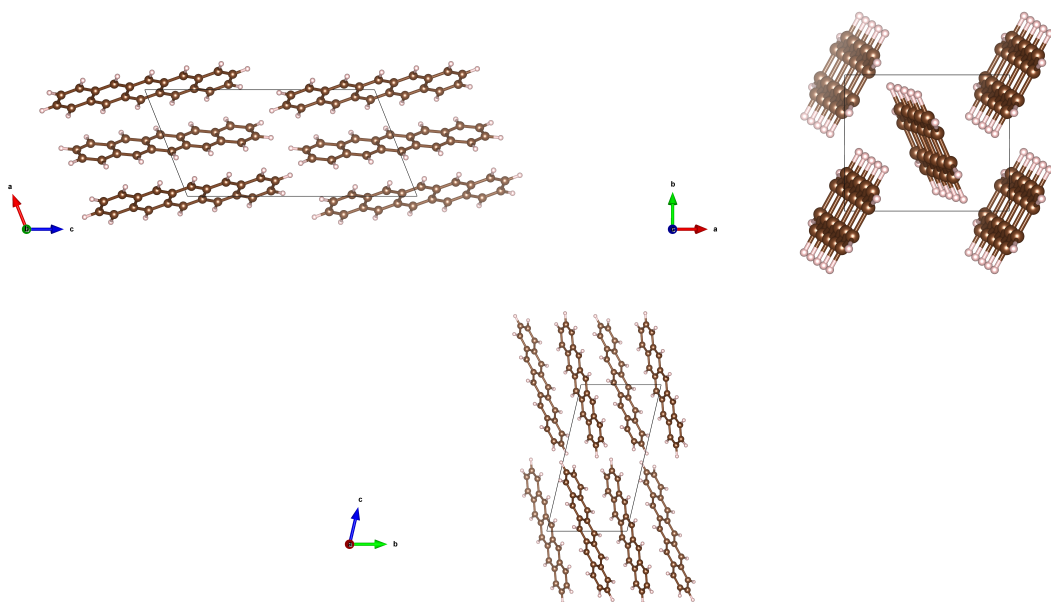
Figure 1.13 – The *ac*, *ab* planes of pentacene polymorph C at the top and *bc* plane of pentacene polymorph H at the bottom

Table 1.18 – Lattice parameters of Pentacene molecule (Polymorphe H) calculated in VASP code

	D2	D3	TS	TS-SCS	PBE*	Exp
<b>a</b>	6.16 (6.18)	6.27	6.13	6.37	6.93	6.27
<b>b</b>	7.25 (7.32)	7.77	7.54	7.68	8.79	7.78
<b>c</b>	13.96 (13.98)	14.48	14.33	14.46	15.36	14.53
$\alpha$	78.99 (78.92)	76.72	77.89	77.62	72.10	76.48
$\beta$	88.69 (90.73)	88.19	87.76	87.66	86.85	87.68
$\gamma$	83.83(83.00)	84.43	84.49	84.42	85.07	84.68
<b>Volume (Å<sup>3</sup>)</b>	608.37 (615.63)	683.04	644.52	687.62	886.39	685.15

\* without dispersion correction

° Parenthesis values were calculated with CRYSTAL program

Table 1.19 – Lattice parameters of pentacene molecule (polymorphe C) calculated in VASP code

	D2	D3	TS	TS-SCS	PBE*	Exp
<b>a</b>	7.40 (7.02)	7.81	7.67	7.61	9.03	7.90
<b>b</b>	5.98 (5.70)	6.09	6.02	6.09	6.54	6.06
<b>c</b>	15.70 (15.68)	15.97	15.82	15.92	16.23	16.01
$\alpha$	102.67 (89.98)	101.97	102.08	101.40	101.91	101.90
$\beta$	113.48 (97.19)	112.31	112.73	112.57	110.91	112.60
$\gamma$	84.98 (90.00)	85.33	85.53	85.63	86.42	85.80
<b>Volume (Å<sup>3</sup>)</b>	622.05 (622.95)	686.75	659.16	668.18	878.28	692.38

\* without dispersion correction

° Parenthesis values were calculated with CRYSTAL program

The second parameter is the one characterising at the same time the chain lengths and “widths”. Calculations for the phenanthrene, pyrene and chrysene molecules were then performed. Furthermore, an additional calculation was performed for the fluorene molecule in order to verify that the signature of the interaction modes does not depend of the nature of the aromatic cycles composing the studied systems. The crystalline structures used for our modelling correspond to those already found in literature for low-pressure room-temperature conditions, *i.e.*, monoclinic P21 [64], monoclinic I2/c [66], monoclinic P21/a [64] and orthorombic Pnam [67], for phenanthrene, chrysene, pyrene and fluorene, respectively. The numerical results so-obtained are reported in Tables 1.20, 1.21, 1.22 and 1.24, and the corresponding crystalline cells are shown in Figures 1.14, 1.15, 1.16 and 1.18 .

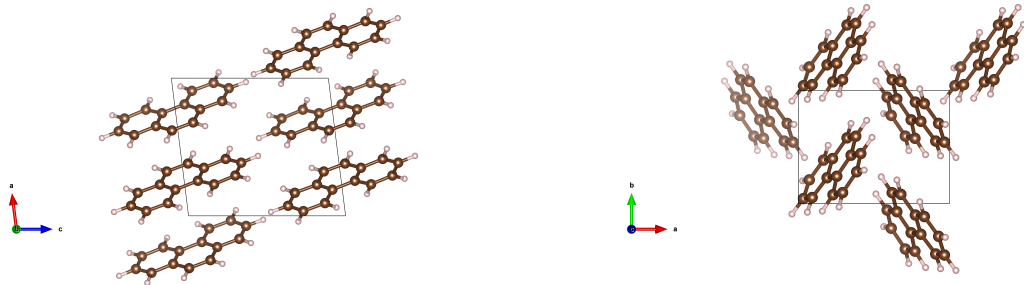
Figure 1.14 – The *ac* and *ab* planes of phenanthrene crystal

Table 1.20 – Lattice parameters of phenanthrene molecule calculated in VASP code

	D2	D3	TS	TS-SCS	PBE*	Exp
<b>a</b>	7.91 (8.61)	8.31	8.12	8.14	9.59	8.47
<b>b</b>	6.04 (5.46)	6.13	6.06	6.09	6.86	6.17
<b>c</b>	9.30 (9.24)	9.44	9.35	9.37	10.08	9.47
$\beta$	95.89 (95.32)	97.18	96.73	96.73	100.43	98.01
<b>Volume (Å<sup>3</sup>)</b>	441.56 (432.83)	477.42	456.69	460.92	651.81	489.72

\* without dispersion correction

○ Parenthesis values were calculated with CRYSTAL program

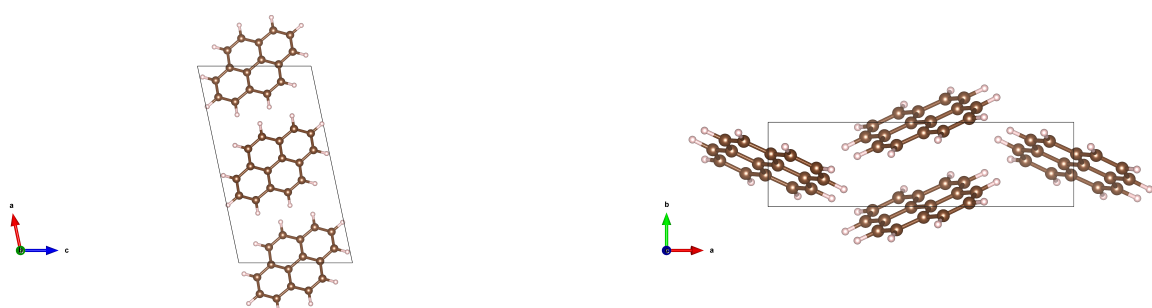
Figure 1.15 – The *ac* and *ab* planes of pyrene crystal

Table 1.21 – Lattice parameters of pyrene molecule calculated in VASP code

	D2	D3	TS	TS-SCS	PBE*	Exp
<b>a</b>	14.64 (13.22)	14.93	15.02	15.10	16.17	15.35
<b>b</b>	3.98 (4.41)	4.04	3.93	4.00	4.64	3.85
<b>c</b>	8.03 (8.01)	8.42	8.43	8.42	9.10	8.65
$\beta$	101.56 (98.28)	101.88	102.02	101.83	103.82	103.03
<b>Volume (Å<sup>3</sup>)</b>	470.08 (461.94)	497.74	487.22	497.70	690.67	498.00

\* without dispersion correction

<sup>0</sup> Parenthesis values were calculated with CRYSTAL program

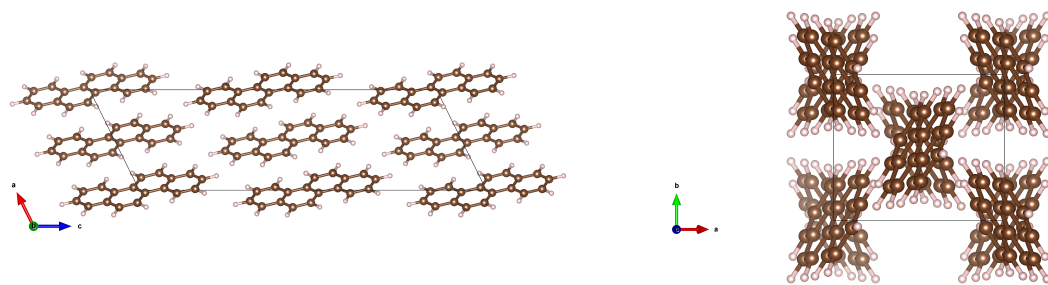
Figure 1.16 – The *ac* and *ab* planes of Chrysene crystal

Table 1.22 – Lattice parameters of chrysene molecule calculated in VASP code

	D2	D3	TS	TS-SCS	PBE*	Exp
<b>a</b>	7.85 (8.67)	8.18	8.13	8.04	9.61	8.39
<b>b</b>	6.08 (5.40)	6.23	6.13	6.13	6.54	6.20
<b>c</b>	25.10 (24.88)	25.39	25.19	25.15	26.10	25.20
$\beta$	117.05 (114.80)	116.39	116.56	116.87	115.76	116.20
<b>Volume (Å<sup>3</sup>)</b>	1067.63 (1057.28)	1157.58	1123.04	1105.90	1476.90	1175

\* without dispersion correction    <sup>0</sup> Parenthesis values were calculated with CRYSTAL program

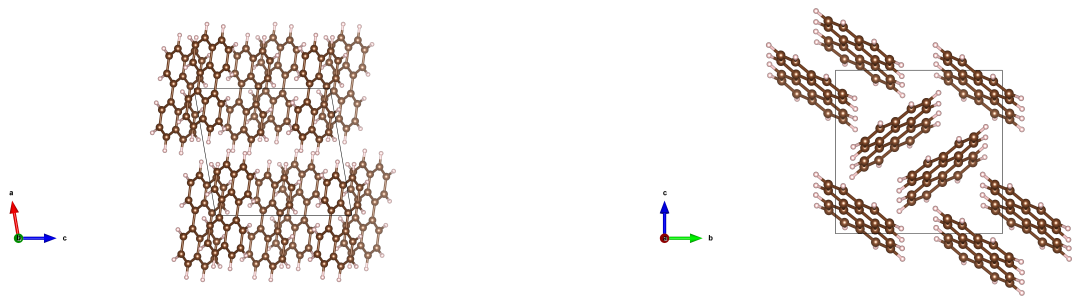
Figure 1.17 – The *ac* and *bc* planes of Perylene crystal

Table 1.23 – Lattice parameters of Perylene molecule calculated in VASP code

	D2	D3	TS	TS-SCS	PBE*	Exp
<b>a</b>	9.99 (10.37)	10.29	10.21	10.27	10.80	10.27
<b>b</b>	10.67 (10.27)	11.00	10.91	10.98	11.41	10.84
<b>c</b>	10.51 (10.91)	10.92	10.64	10.83	12.85	11.28
$\beta$	99.54 (103.62)	99.70	99.25	99.55	102.75	100.53
<b>Volume (Å<sup>3</sup>)</b>	1105.54 (1128.72)	1218.72	1169.03	1203.94	1544.16	1234.29

\* without dispersion correction      <sup>0</sup> Parenthesis values were calculated with CRYSTAL program

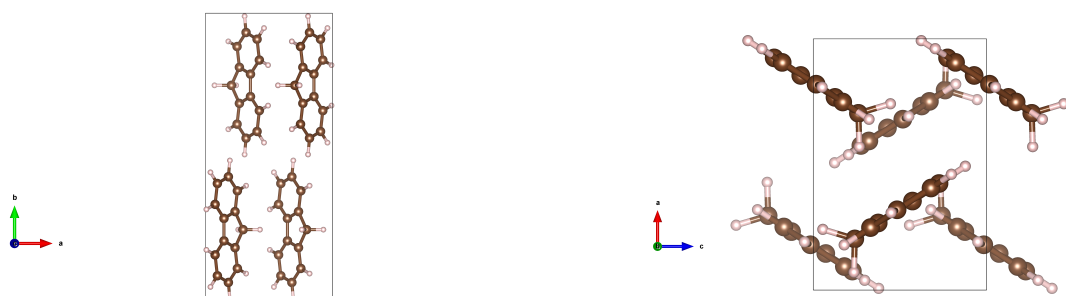
Figure 1.18 – The *ab* and *ac* planes of fluorene crystal

Table 1.24 – Lattice parameters of Fluorene molecule calculated in VASP code

	D2	D3	TS	TS-SCS	PBE*	Exp
<b>a</b>	7.96 (8.25)	8.30	8.08	8.16	9.77	8.48
<b>b</b>	18.40 (18.61)	18.90	18.77	18.82	19.54	18.92
<b>c</b>	5.54 (5.26)	5.72	5.64	5.68	6.16	5.72
<b>Volume (Å³)</b>	810.91 (807.12)	897.69	855.73	871.59	1176.23	916.60

\* without dispersion correction

( ) Parenthesis values were calculated with CRYSTAL program

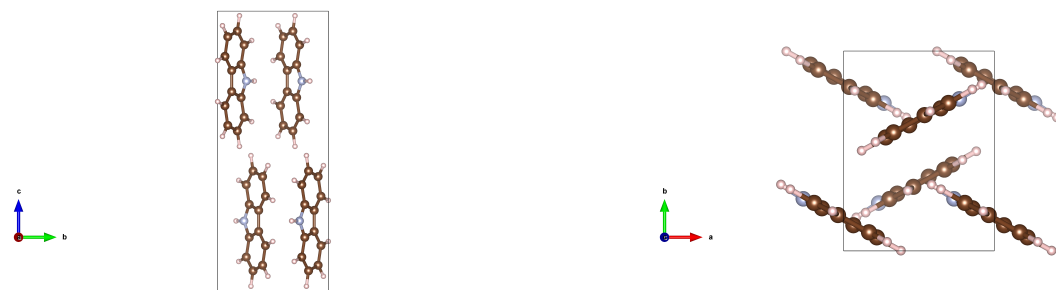
Figure 1.19 – The *bc* and *ab* planes of Carbazole crystal

Table 1.25 – Lattice parameters of Carbazole molecule calculated in VASP code

	D2	D3	TS	TS-SCS	PBE*	Exp
<b>a</b>	5.59 (5.51)	5.77	5.70	5.70	6.07	5.71
<b>b</b>	7.27 (7.21)	7.64	7.39	7.44	8.67	7.78
<b>c</b>	18.75 (18.86)	19.20	19.08	19.07	19.67	19.11
<b>Volume (Å³)</b>	762.34 (749.46)	846.60	804.18	808.71	1035.61	848.88

\* without dispersion correction

( ) Parenthesis values were calculated with CRYSTAL program

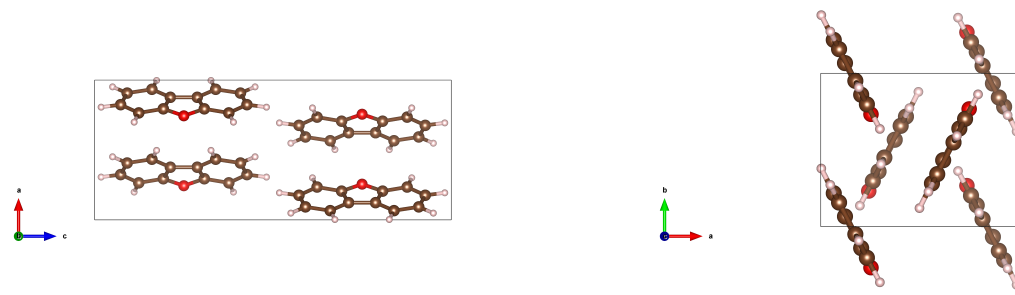
Figure 1.20 – The *ac* and *bc* planes of Dibenzofuran crystal

Table 1.26 – Lattice parameters of Dibenzofuran molecule calculated in VASP code

	D2	D3	TS	TS-SCS	PBE*	Exp
<b>a</b>	7.17 (6.94)	7.52	7.36	7.34	8.68	7.70
<b>b</b>	5.69 (5.65)	5.86	5.78	5.79	6.29	5.83
<b>c</b>	18.84 (20.26)	19.22	19.05	19.08	19.81	19.19
<b>Volume (Å³)</b>	769.27 (793.69)	847.16	810.05	810.10	1082.30	860.72

\* without dispersion correction

○ Parenthesis values were calculated with CRYSTAL program

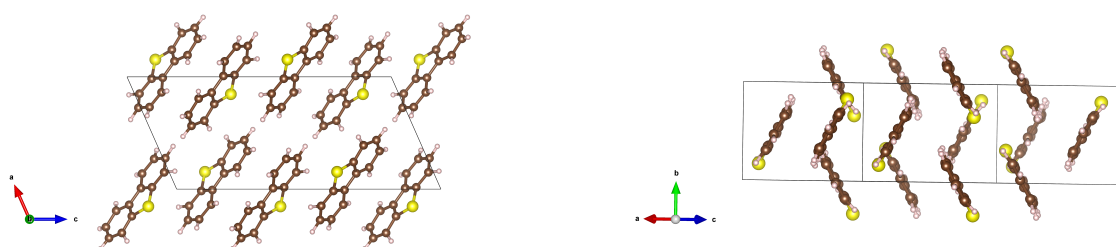
Figure 1.21 – The *ac* plane and other view of molecular arrangement of Dibenzothiophene crystal

Table 1.27 – Lattice parameters of Dibenzothiophene molecule calculated in VASP code

	D2	D3	TS	TS-SCS	PBE*	Exp
<b>a</b>	8.26 (8.59)	8.56	8.36	8.54	9.83	8.67
<b>b</b>	5.86 (5.68)	6.03	5.95	6.05	6.48	6.00
<b>c</b>	17.94 (17.83)	18.44	18.04	18.39	20.95	18.70
$\beta$	111.54 (112.66)	112.07	111.87	111.79	119.32	113.90
<b>Volume (Å<sup>3</sup>)</b>	808.18 (802.53)	882.92	847.06	883.16	1163.07	889.36

<sup>\*</sup> without dispersion correction<sup>(*o*)</sup> Parenthesis values were calculated with CRYSTAL programTable 1.28 – Calculated vibrational frequencies (cm<sup>-1</sup>) of the monomer, dimer and solid-state (PBE Benzene system).

Assignment	Monomer		Dimer		Experimental		VASP/CRYSTAL	
	$\nu$ (cm <sup>-1</sup> )	Int(km/mol)	$\nu$ (cm <sup>-1</sup> )	Int(km/mol)	$\nu$ (cm <sup>-1</sup> )		$\omega$ (cm <sup>-1</sup> )	Int(km/mol)
$\nu_1$	7 (0.04)							
	12 (<0.01)							
	48 (<0.01)							
	56 (0.07)							
	63 (0.08)						63 (0.69)	
	75 (0.03)						71 (0.05)	
							101 (0.69)	
							119 (4.24)	
							126 (1.11)	
							128 (4.83)	
							410 (0.05)	
							419 (0.79)	

Italic: Intermolecular modes

Table 1.29 – Calculated vibrational frequencies ( $\text{cm}^{-1}$ ) of the monomer, dimer and solid-state (PBE Naphthalene system).

Monomer		Dimer	Experimental ref [58] $\nu(\text{cm}^{-1})$	VASP/CRYSTAL $\omega(\text{cm}^{-1})$ Int(km/mol)
Assignment	$\nu(\text{cm}^{-1})$ Int(km/mol)	$\nu(\text{cm}^{-1})$ Int(km/mol)		
		33 (0.04) 36 (0) 55 (0) 75 (0.21) 88 (0.08) 101 (0)		
$\nu_1$	177 (3.2)	181 (3.8) 188 (0) 201 (1.2)	176	174 (2.60)
$\nu_2$	191 (0)	201 (0)	195	190 (0.04) 208 (0.03) 210 (1.26)
$\nu_3$	379 (1.5)	372 (2.2) 372 (0)	359	362 (0.35) 364 (1.54)
$\nu_4$	403 (0)	396 (0.02)		386 (0) 391 (0)

Italic : Intermolecular modes

Table 1.30 – Calculated vibrational frequencies ( $\text{cm}^{-1}$ ) of the monomer, dimer and solid-state (PBE Anthracene system).

<b>Monomer</b>		<b>Dimer</b>	<b>Experimental</b> ref [68]/ ref [69]	<b>VASP/CRYSTAL</b>
Assignment	$\nu(\text{cm}^{-1})$ Int(km/mol)	$\nu(\text{cm}^{-1})$ Int(km/mol)	$\nu(\text{cm}^{-1})$	$\omega(\text{cm}^{-1})$ Int(km/mol)
		22 (0.004) 34 (0) 57 (0) 75 (0.05) 87 (0.8)	63 m 72 w	98(1.37)
$\nu_1$	93 (1.5)	111 (0.8) 112 (1.2)	106/104 m 110 s	101 (4.03) 119 (0.05)
$\nu_2$	124 (0)	148 (0.6) 149 (0.02)	137/126 s 166 s	153 (1.77) 155 (0.07)
$\nu_4$	243 (1.4)	244 (2.1) 244 (0)	234/235 s	239 (1.25) 239 (0.33)
$\nu_5$	276 (1.1)	250 (0) 253 (0.2)	244	236 (0) 237 (0)
		285 (0.02) 286 (0.08)	287	278 (0) 281 (0)
$\nu_6$	394 (0.05)	396 (0.2) 396 (0.04)	380/361vw 380 w	375 (0.23) 379 (0.36)
$\nu_7$	407 (0)	407 (0) 407 (0.04)	397	389 (0) 391 (0)

Italic: Intermolecular modes

Table 1.31 – Calculated vibrational frequencies ( $\text{cm}^{-1}$ ) of the monomer, dimer and solid-state (PBE Pentacene system).

Monomer	Dimer	Experimental (P.A.) ref [70]	VASP/CRYSTAL
Assignment	$\nu(\text{cm}^{-1})$ Int(km/mol)	$\nu(\text{cm}^{-1})$ Int(km/mol)	$\omega(\text{cm}^{-1})$ Int(relative)
	19 ( $<0.01$ ) 27 (0.0) 38 (0.5)	42 (0.4) 57 (0.0) 72 (0.9) 74 (0.07) 84 (0) 95 (0.0)	58 (0.46)
$\nu_3$	97(0.003)	101 (0.002) 108 (0.2)	102 (m)  102 (5.17)
$\nu_4$	122 (1.0)	122 (1.5)  125 (0.0) 130 (0.08)	122 (m)  117 (0.99) 127 (0.21)  134 (6.1)
$\nu_1 + \nu_3$	144 (0.04)		141 (m)  140 (0.68) 148 (1.58)
$\nu_2 + \nu_3$	164( $<0.01$ )	168 (0.2) 168 (0.05)	165 (vw)  188 (w) 198 (m)  180 (2.54)
$\nu_6$	194 (1.4)	204 (2.2)	204 (2.36)
$\nu_3 + \nu_4$	224 (0.0)	210(0.002)	223 (vw)
$\nu_2 + \nu_5$	222 (0.002)		
$\nu_1 + 2\nu_3$	251 (0.0)	247 (0.05)	254 (0.29)
$\nu_9$	265 (0.03)	255 (0.02)	257 (w)
$2\nu_1 + \nu_6$	274 ( $<0.01$ )		272 (vw)  272 (0.45)
$\nu_3 + \nu_6$	291 ( $<0.01$ )	302 (0.005)	296 (w)
$\nu_1 + \nu_9$	292 ( $<0.01$ )	303 (0.07)	
$\nu_2 + \nu_7$	316 ( $<0.01$ )		317 (w)
$\nu_3 + \nu_8$	346 (0.03)		344 (vw)
$\nu_{12}$	374 (0.1)		352 (1.12) 355 (0.27)
$\nu_{13}$	374 (0.03)		382 (0.01) 386 (0.34)

Italic: Intermolecular modes

Table 1.32 – Calculated vibrational frequencies ( $\text{cm}^{-1}$ ) of the monomer, dimer and solid-state (PBE Phenanthrene system).

Monomer		Dimer	Experimental ref [71]/ ref [72]	VASP/CRYSTAL
Assignment	$\nu(\text{cm}^{-1})$ Int(km/mol)	$\nu(\text{cm}^{-1})$ Int(km/mol)	$\nu(\text{cm}^{-1})$	$\omega(\text{cm}^{-1})$ Int(km/mol)
		<i>11 (0.003)</i>		
		<i>14 (0.005)</i>		
		<i>42 (0.02)</i>		<i>57 (0.4)</i>
		<i>69 (0.2)</i>		<i>63 (1.05)</i>
		<i>74 (0.06)</i>		<i>73 (0.01)</i>
		<i>81 (0.02)</i>	89	<i>88 (0.91)</i>
				<i>93 (1.88)</i>
$\nu_1$	99 (0)	102 (1.04) 113 (0.61)	97	103 (0.34) 118 (1.88)
$\nu_2$	103 (1.06)	123 (0.44) 126 (0.02)	124/127 143 sh	119 (0.05) 127 (0.53)
$\nu_3$	235 (5.01)	239 (9.23) 244 (0.35)	229(w)/233s	231 (0.44) 241 (0.86)
$\nu_4$	251 (0)	250 (0.31) 255 (0.5)		241 (0.12) 243 (4.21)
$\nu_5$	255 (0.43)	255 (0.21) 259 (0.13)	248(s)/250m 289(w)	250 (2.51) 251 (0.04)
$\nu_6$	412 (0)	411 (0.03) 415 (0.28)	409(w)/408ms	394 (0.34) 395 (0.11) 403 (0.1) 408 (0.63)

Italic: Intermolecular modes

Table 1.33 – Calculated vibrational frequencies ( $\text{cm}^{-1}$ ) of the monomer, dimer and solid-state (PBE Pyrene system).

	<b>Monomer</b>	<b>Dimer</b>	<b>Experimental</b> ref [73]	<b>VASP/CRYSTAL</b>
Assignment	$\nu(\text{cm}^{-1})$ Int(km/mol)	$\nu(\text{cm}^{-1})$ Int(km/mol)	$\nu(\text{cm}^{-1})$	$\omega(\text{cm}^{-1})$ Int(km/mol)
		<i>17 (&lt;0.01)</i>		
		<i>30 (0)</i>		
		<i>40 (0)</i>		
		<i>69 (0.01)</i>		<i>50 (0.05)</i>
		<i>94 (0.01)</i>	83 (m)	<i>94 (5.98)</i>
		<i>95 (0)</i>		
$\nu_1$	100 (0.66)	115 (1.60)	98 (m)	<i>97 (2.31)</i> 105 (0.33)
			121 (w)	
			138 (vw)	135 (2.71)
$\nu_2$	157 (0)	162 (0.03)	157 (w)	<i>157 (0.77)</i> 162 (4.27)
			181 (vw)	
			197 (vw)	
$\nu_3$	220(12.56)	225(24.34)	221 (m)	<i>211 (4.64)</i> 231 (7.89)
$\nu_4$	260 (0)	<i>264 (0)</i>	260 (w)	<i>261 (0)</i>
$\nu_5$	269 (0)	275 (0.18)	284 (w) 305 (vw) 323 (w)	<i>264 (0)</i>
$\nu_6$	370 (1.54)	370 (2.05)	353 (m)	<i>349 (0.53)</i> 350 (1.71)
$\nu_7$	412 (0)	416(0.004)	396 (vw)	<i>391 (0.82)</i> 394 (0.04)

Italic: Intermolecular modes

Table 1.34 – Calculated vibrational frequencies ( $\text{cm}^{-1}$ ) of the monomer, dimer and solid-state (PBE Chrysene system).

	<b>Monomer</b>	<b>Dimer</b>	<b>Experimental</b> ref [74]	<b>VASP/CRYSTAL</b>
Assignment	$\nu(\text{cm}^{-1})$ Int(km/mol)	$\nu(\text{cm}^{-1})$ Int(km/mol)	$\nu(\text{cm}^{-1})$	$\omega(\text{cm}^{-1})$ Int(km/mol)
$\nu_1$	50 (0.21)	15 (0.002) 26 (0.02) 34 (0)		41 (0.01) 69 (0.11)
$\nu_2$	79 (0.34)	53 (0.2) 76 (0.02) 86 (0) 88 (0.18) 95 (0.95)		112 (2.88) 114 (3.19)
$\nu_3$	138 (0)	100 (0) 115 (0) 145 (0) 157 (0.01)		100 (0.09) 134 (0.63) 158 (0.26)
$\nu_4$	181 (0)	190 (0) 194 (0.13)		
$\nu_5$	192 (0.52)	194 (0.73) 195 (0)		189 (0.82)
$\nu_6$	243 (7.50)	248 (14.70) 254 (0)	232	247 (1.18) 251 (10.72)
$\nu_7$	300 (0)	302 (0) 303 (0.06)		
$\nu_8$	301 (0.24)	308 (0) 309 (0.44)		292 (2.56) 295 (0.09)
$\nu_9$	396 (0)	396 (0.005) 396 (0)		

Italic: Intermolecular modes

Table 1.35 – Calculated vibrational frequencies ( $\text{cm}^{-1}$ ) of the monomer, dimer and solid-state (PBE Perylene system).

Monomer		Dimer	Experimental ref [73]	VASP/CRYSTAL
Assignment	$\nu(\text{cm}^{-1})$ Int(km/mol)	$\nu(\text{cm}^{-1})$ Int(km/mol)	$\nu(\text{cm}^{-1})$	$\omega(\text{cm}^{-1})$ Int(km/mol)
$\nu_1$	17 (0.00)	14 (0.001) 33(0.00) 31 (0.00) 35 (0.00) 73 (0.10) 84 (0.15) 89 (0.00)		39 (0.12) 45 (0.06) 48 (0.17) 87 (3.61)
$\nu_2$	100 (1.00)	110 (2.00) 126 (0.00)	98 (m)	95 (0.29) 103 (1.03) 104 (9.86) 111 (7.38) 117 (m)
$\nu_3$	128 (0.00)	138 (0.00) 144 (0.08)	124 (vw) 142 (w) 157 (w)	127 (0.52) 148 (0.68) 152 (1.73) 185 (1.10)
$\nu_4$	182 (8.02)	190 (15.52) 192 (0.00)	185 (m)	187 (16.72) 189 (0.55)
$\nu_5$	212 (0.00)	218 (0.00) 223 (0.02)	205 (vw) 222 (vw)	219 (0.00) 233 (0.06)
$\nu_6$	245 (0.00)	249 (0.09) 253 (0.00)	254 (w)	244 (0.03) 249 (0.20) 250 (0.01)
$\nu_7$	264 (0.19)	264 (0.00) 264 (0.27)	283 (vw)	299 (0.02) 300 (0.62)
$\nu_8$	307 (0.00)	312 (0.00) 315 (0.72)	311 (vw) 323 (vw)	348 (0.04) 350 (0.06)
$\nu_9$	366 (0.00)	367 (0.00) 367 (0.04)	354 (w)	361 (0.13) 363 (0.14)
$\nu_{10}$	375 (0.00)	375 (0.00) 375 (0.04)	395 (vw)	410 (0.31)

Italic: Intermolecular modes

Table 1.36 – Calculated vibrational frequencies ( $\text{cm}^{-1}$ ) of the monomer, dimer and solid-state (PBE Fluorene system).

Monomer		Dimer	Experimental ref [75] $\nu(\text{cm}^{-1})$	VASP/CRYSTAL $\omega(\text{cm}^{-1})$ Int(km/mol)
Assignment	$\nu(\text{cm}^{-1})$ Int(km/mol)	$\nu(\text{cm}^{-1})$ Int(km/mol)		
		20 (0.01) 23 (0.06) 35 (0.02) 74 (0.06) 85 (0.1) 89 (0.02)		
$\nu_1$	100 (0.84)	119 (1.16) 124 (0.02)	108 (m) 122 (w)	100 (5.17) 101 (2.18) 110 (1.13) 118 (0.83)
$\nu_2$	140 (0)	148 (0.04) 162 (0.04)	140 (w)	123 (0.93)
$\nu_3$	220 (0.22)	221 (0.18) 222 (0.17)	217 (m)	160 (0.02) 222 (0.04) 226 (2.87)
$\nu_4$	254 (9.39)	265 (6.20) 277 (16.91)	256 (m) 266 (m)	248(14.23) 262 (42.37) 266 (0.01)
$\nu_5$	286 (0)	292 (0.04) 297 (0.11)	302 (w)	
$\nu_6$	429 (0.45)	430 (0.54) 430 (0.23)	411 (s)	405 (9.39) 405 (4.71)
$\nu_7$	439 (8.29)	440 (19.00) 442 (1.09)		407(19.44)

Italic: Intermolecular modes

Table 1.37 – Calculated vibrational frequencies ( $\text{cm}^{-1}$ ) of the monomer, dimer and solid-state (PBE Carbazole system).

Monomer		Dimer	Experimental	VASP/CRYSTAL
Assignment	$\nu(\text{cm}^{-1})$ Int(km/mol)	$\nu(\text{cm}^{-1})$ Int(km/mol)	$\nu(\text{cm}^{-1})$ Fig	$\omega(\text{cm}^{-1})$ Int(km/mol)
		26 (0.05) 31 (0.03) 43 (0.02) 65 (1.32) 70 (0.01) 95 (0.51)	71 (w)	66 (0.13) 72 (13.88)
$\nu_1$	103 (5.54)	115 (2.85) 158 (0.11)	125 (m)	112 (0.86) 114 (3.31) 118 (26.62)
$\nu_2$	150 (0.00)	153 (0.12) 168 (0.04)	146 (w)	142 (8.41)
$\nu_3$	222 (0.38)	221 (0.47) 221 (0.35)	221 (m)	185 (0.49) 221 (0.26) 222 (0.52)
$\nu_4$	284(15.47)	301 (0.74) 305 (0.01)	294 (w)	283 (0.43)
$\nu_5$	297 (0.00)	321 (0.02) 325 (2.83)	312 (w)	303 (9.96) 309 (12.45)
$\nu_6$	344(61.71)			
$\nu_7$	434(11.32)	431 (7.50) 438 (11.67)	423 (s)	418 (63.87) 419 (6.27)
$\nu_8$	439 (1.44)	435 (5.64) 436 (77.40)		428 (0.78)
		446 (203.89) 447 (30.18)	445 (s)	434(43.81)
$\nu_5$	453 (0.00)	457 (13.23) 458 (0.02)		441 (1.34)

Italic: Intermolecular modes

Table 1.38 – Calculated vibrational frequencies ( $\text{cm}^{-1}$ ) of the monomer, dimer and solid-state (PBE Dibenzofuran system).

Monomer		Dimer	Experimental ref [76]	VASP/CRYSTAL
Assignment	$\nu(\text{cm}^{-1})$ Int(km/mol)	$\nu(\text{cm}^{-1})$ Int(km/mol)	$\nu(\text{cm}^{-1})$	$\omega(\text{cm}^{-1})$ Int(km/mol)
		12 (0.03) 27 (0.04) 37 (0.09) 63 (0.06) 78 (0.26) 88 (0.08)		
				53 (1.83) 78 (0.01)
$\nu_1$	105 (2.18)	121 (4.03) 126 (0.04)	103	106 (3.86) 108 (0.75) 117 (1.09)
$\nu_2$	152 (0.00)	163 (0.04) 167 (0.06)	150	140 (0.47) 152 (0.14)
$\nu_3$	222 (1.19)	222 (0.34) 222 (1.52)	217	217 (0.42) 221 (2.86)
$\nu_4$	294 (0.00)	299 (0.05) 302 (0.11)	287	286 (0.01)
$\nu_5$	317 (0.01)	321 (0.28) 323 (0.02)	310	314 (0.22) 317 (1.27)
$\nu_6$	434 (6.24)	434 (10.51) 437 (2.71)	419	413 (1.65) 434 (26.52)
$\nu_7$	434 (1.88)	436 (1.41) 436 (1.47)	424	425 (6.91)

Italic: Intermolecular modes

Table 1.39 – Calculated vibrational frequencies ( $\text{cm}^{-1}$ ) of the monomer, dimer and solid-state (PBE Dibenzothiophene system).

Monomer		Dimer	Experimental Table	VASP/CRYSTAL
Assignment	$\nu(\text{cm}^{-1})$ Int(km/mol)	$\nu(\text{cm}^{-1})$ Int(km/mol)	$\nu(\text{cm}^{-1})$	$\omega(\text{cm}^{-1})$ Int(km/mol)
		18 (0.05) 28 (0.01) 36 (0.09) 70 (0.32) 89 (0.01) 93 (0.56)		
			49 (0.38) 80 (1.86) 84 (0.07) 91 (2.43) 99 (0.47) 108 (0.60) 113 (2.61)	
$\nu_1$	102 (1.54)	118 (2.14) 128 (0.06)	135 (m)	138 (0.03) 140 (1.14)
$\nu_2$	135 (0.00)	147 (0.04) 162 (0.10)		163 (0.45) 172 (0.39)
$\nu_3$	217 (0.85)	217 (0.29) 217 (1.09)	213 (m)	213 (2.52) 215 (5.04)
$\nu_4$	221 (1.46)	231 (3.05) 235 (0.07)	228 (m)	229 (1.93) 230 (3.94)
			269 (vw)	
$\nu_5$	279 (0.00)	286 (0.01) 289 (0.13)	282 (vw)	278 (0.39) 283 (0.11)
$\nu_6$	416 (2.83)	416 (0.24) 416 (4.21)	404 (s)	404 (8.59) 406 (0.39)
				415 (6.30)
$\nu_7$	428 (0.15)	428 (0.24) 429 (0.08)	419 (sh)	416 (0.60) 418 (0.24)
$\nu_8$	433 (7.15)	433 (16.66) 435 (0.23)	425 (s)	423 (18.48) 435 (3.29)

Italic: Intermolecular modes

The results associated to the acene family, i.e., naphthalene, anthracene and pentacene, are reported in Tables 1.29, 1.30 and 1.31 hereafter. The calculation conditions in this piece of modelling are identical to those used just before for the tetracene molecule. The main conclusions arising from the study of these systems are in agreement with those obtained for the tetracene system. Indeed, for these three systems, the structural parameters and unit cell volumes are better described by the PBE-D3 level of theory if a comparison is made with the other methods used in this work (except for the two anthracene and benzene systems where the TS and the TSC data are in relative better agreement in comparison to the experimental data [77]. The

agreement between our theoretical and experimental data meets the requirements to the frequency calculation of the crystalline network. Moreover, the inclusion of the dispersive terms (like D3 or the modified D2:TS) must be introduced onto the frequency calculation because of the well-known dispersive character of the intermolecular modes to describe. The vibrational results calculated for these systems are reported in Table 1.28, 1.29, 1.30, 1.31, 1.32, 1.33, 1.34 and 1.36 in which the frequency values can also be found for each acene family-member monomer and dimer. According to the conclusions drawn for the tetracene system case, one can find for these three systems at least an active signature associated to a network vibrational mode around  $100\text{ cm}^{-1}$  ( $88$  and  $106\text{ cm}^{-1}$  for naphthalene,  $98\text{ cm}^{-1}$  for anthracene, and  $102\text{ cm}^{-1}$  for pentacene). One should note that the benzene molecule (also in the acene family) in its T-Shape conformation needs a specific analysis. As a matter of fact, for this conformation, the intermolecular interactions of the crystal network do not correspond any longer to the simple pi-pi interactions (as it is the case of the other systems herein studied) but to interactions of the type pi-H, as demonstrated by Katrusiak et coll [63]. Yet, although the interactions are of different nature, our calculations show that the main active vibrational signature of the crystalline network remains localised in the  $100\text{-}130\text{ cm}^{-1}$  region. Moreover, in the following paragraphs, it will be shown that the spectral position remains unchanged for different systems only for this (these) specific mode(s). For all the other modes, depending on the symmetry of the system and on the strength of the long-range interactions between neighbour molecules, the spectral signatures can vary in position and in intensity. This observation only constitutes the major information to be extracted from our calculations given the aim of this work. The vibrational data obtained within the same calculation conditions for the polyaromatic phenanthrene, pyrene and chrysene molecule lead to the same conclusions: each system owns at least one active signature found around  $100\text{ cm}^{-1}$  and inherent to the network ( $88$  and  $106\text{ cm}^{-1}$  for phenanthrene,  $94$  and  $97\text{ cm}^{-1}$  for pyrene,  $112$  and  $114\text{ cm}^{-1}$  for chrysene). The fluorene molecule, besides having a different aromatic constitution (other than benzenic rings) lead to the similar results, for which the modes were estimated to be found at  $88$  and  $100\text{ cm}^{-1}$ .

The available vibrational data for these nine systems are not easily exploitable for the network modes characterization. For these modes, indeed, either the data is incomplete or the intramolecular signatures (highlighted by the calculations of the monomers) overlap the intermolecular ones in the  $100\text{-}150\text{ cm}^{-1}$  zone. For example, the modes associated to pyrene (monomer calc  $100\text{ cm}^{-1}$  int  $0.66\text{ km.mol}^{-1}$  – solid state calc  $97\text{ cm}^{-1}$  int  $2.31\text{ km.mol}^{-1}$ ) and fluorene (monomer calc  $100\text{ cm}^{-1}$  int  $0.84\text{ km.mol}^{-1}$  – solid state calc  $100\text{ cm}^{-1}$  int  $5.71\text{ km.mol}^{-1}$ ) are respectively measured at  $98$  and  $108\text{ cm}^{-1}$ , illustrating this problem. The tetracene molecules case differs since, as indicated in Table 1.14, the isolated tetracene molecule strictly owns a single signature in the zone of study ( $93\text{ cm}^{-1}$ ) that could potentially hide the network's one. Nevertheless, as the intensity of this mode for the monomer is expected to be zero accordingly to our calculations, one should not have problems assigning it. Even though, as previously, assigning these network modes remains a difficult task and one cannot assure that this single network mode (calc  $102\text{ cm}^{-1}$  int  $2.1\text{ km.mol}^{-1}$ ) corresponds undoubtedly to the one observed experimentally at  $106\text{ cm}^{-1}$ . Notably, since an active mode (int  $9.5\text{ km.mol}^{-1}$ ) of the monomer was also found at  $106\text{ cm}^{-1}$  in the solid state calculations, one should be prudent to interpret such results. Occasional overlap of two vibrators is then a limiting factor for our capability to identify the nature of these observed vibrators in some cases. Still, this fact does not question the presence of these active network modes that we intend to identify, neither the fact that these modes can always be associated to one or two intermolecular vibrations invariably found between  $90$  and  $120\text{ cm}^{-1}$  regardless of the system in study. Third, the same

type of vibrational data is still not available for the benzene, naphthalene, phenanthrene and chrysene molecules.

Anyhow, our calculations can lead experimentalists to locate the presence or not of intramolecular interactions at very low wavenumbers under any given condition (P, T, concentration, . . .). Noteworthy, only the 70-150 cm<sup>-1</sup> zone is herein commented since it is where the signatures we intend to identify are located. Notwithstanding, for the ensemble of systems, the calculated data presented in Tables 1.24-31 were also extended to englobe the 150-400 cm<sup>-1</sup>, allowing in this way both the validation of our calculations in a better experimentally identified zone and the identification of the specific modes of the ‘non interacting’ modes. As such, the solid state calculations herein performed are generally in a very good agreement with the available experimental data. This also contributes to the validation of our results using the same calculation conditions for the regions below 150 cm<sup>-1</sup>.

## Conclusions

The DFT calculations presented in this work provide detailed and accurate descriptions of experimental photoacoustic far IR spectra for tetracene and pentacene and for far IR spectra of the acene family as a whole. The impacts of molecular distortion on monomer and dimer spectra and dimer stability, and the interpretation of peaks in photoacoustic IR spectra of crystalline solids are discussed in detail. Distortion breaks molecular symmetry and this adds to the complexity of the interpretation of the resulting spectra. Inter- and intramolecular vibrations in the acene family of compounds are discriminated, and combinations of inter- and intramolecular vibrations are identified specially with the use of solid-state conditions. Peak assignment ambiguity, and the potential impacts of molecular distortion on peak intensity are addressed for tetracene and pentacene. By examining computed and experimental spectra for the family of acene molecules concurrently, trends in vibration modes with molecular size were used to reinforce assignments, and to reattribute assignments made previously in the experimental tetracene and pentacene spectra. In particular, both dimer and solid state calculations permitted re-assignment of an infrared active peak arising in tetracene at 142 cm<sup>-1</sup> and assignment of large infrared active peaks at 117 and 108 cm<sup>-1</sup> for tetracene and pentacene respectively that may permit their identification in an acene mixture. The intermolecular vibrations for naphthalene, anthracene, tetracene and pentacene, are found in the same wavelength range of the far infrared spectrum and are not readily discriminated one from the other. The specificity of the acene  $\pi$ -stacking interactions, reinforced by calculations with distorted dimers (and solid-state), allows not only the identification of this family of molecules, but also highlights the presence of  $\pi$ -stacking interaction in a mixture as a whole.

If our previsions turn out to be generalizable for all kind of molecular families and molecules, this could give experimentalists an additional tool of characterisation to identify the presence of systems more or less associated and interacting by means of pi-pi or pi-H interactions in the solid state. This work is a complement of the work already performed concerning the characterisation of the H-bond interactions in asphaltene systems (ref DM Hugo). In this way, we believe to be henceforth capable of disposing all the vibrational pieces of information concerning the three potential types of interactions present in the asphaltenic medium and provide, in this way, experimentalists a way to find out the nature of the interactions present in petroleum fluids and their residues and, to a lesser extent, to identify the chemical nature of oil’s constituents.

## Supplementary Data

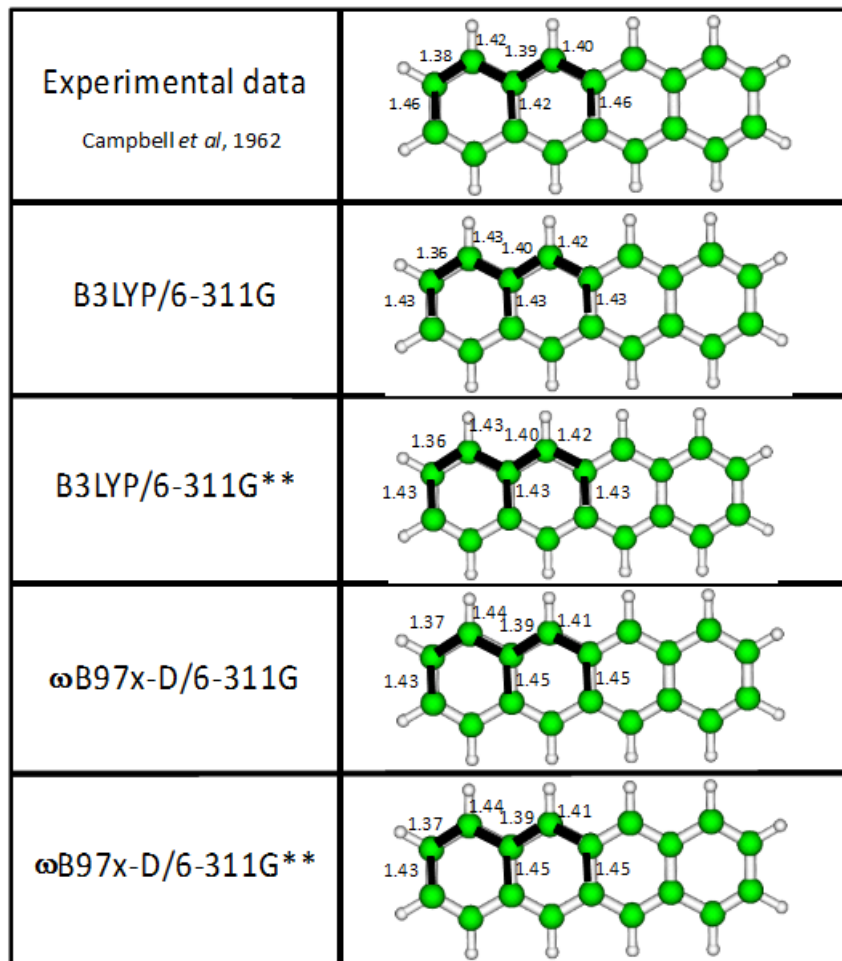


Figure 1.22 – Geometrical data for a tetracene molecule by Campbell et al [4] and values optimized in the framework of various DFT calculations, used in this work

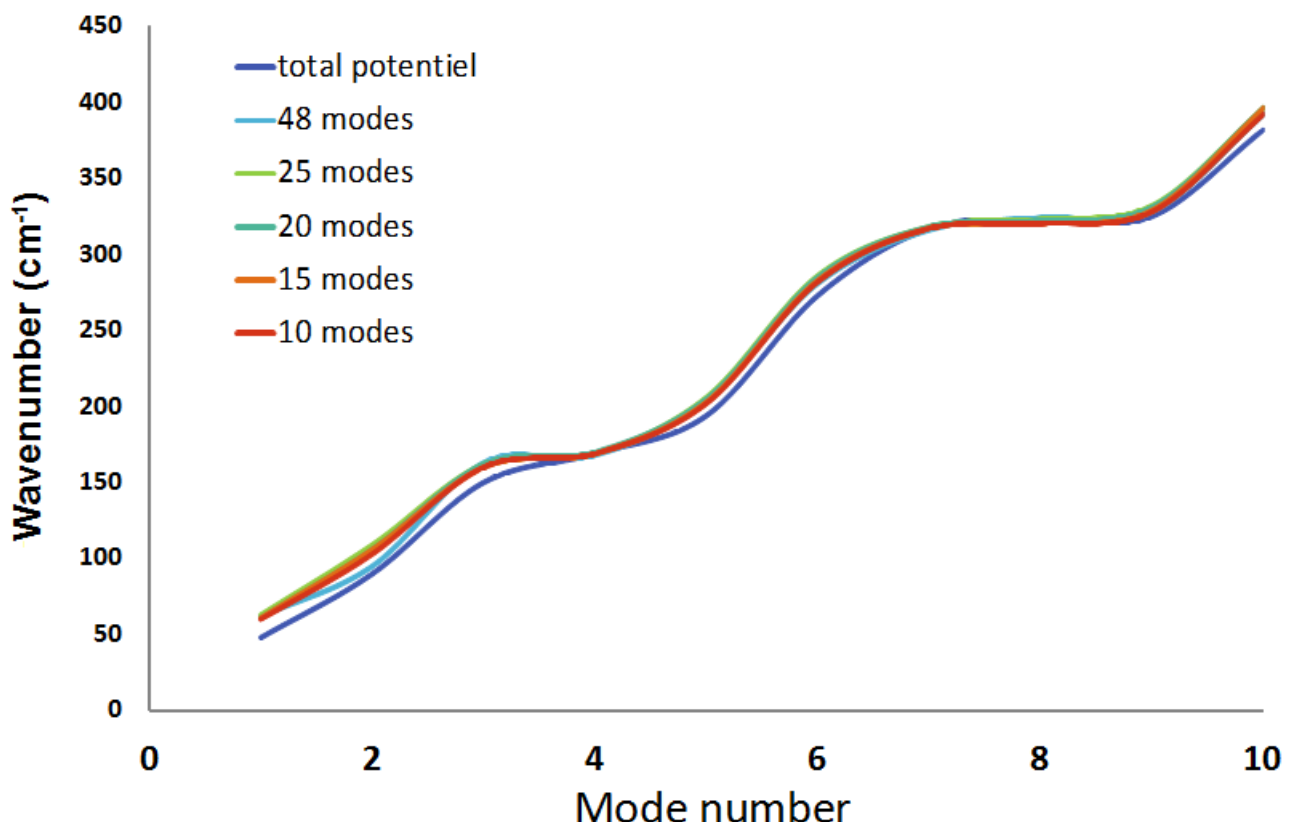


Figure 1.23 – Effect of mode truncature on the wavenumber obtained using  $\omega$ B97X-D/6-311G for the first ten vibration modes of a tetracene molecule, with force truncature ( $f > 5 \text{ cm}^{-1}$ )

Table 1.40 – Computed wavenumbers and intensities for distorted tetracene based on the harmonic approximation at the  $\omega$ B97X-D/6-311G level of calculation. Comparison with symmetric tetracene ( $D_{2h}$ )

Mode	Tetracene with $D_{2h}$ symmetry		Distorted Tetracene	
	Harmonic wavenumber ( $\text{cm}^{-1}$ )	Harmonic Intensity ( $\text{km} \cdot \text{mol}^{-1}$ )	Harmonic wavenumber ( $\text{cm}^{-1}$ )	Harmonic Intensity ( $\text{km} \cdot \text{mol}^{-1}$ )
$\nu_1$	57	0.86	58	0.87
$\nu_2$	93	0	93	0.03
$\nu_3$	154	0	154	0.01
$\nu_4$	168	1.24	168	1.22
$\nu_5$	196	0	196	0.05
$\nu_6$	276	1.03	276	1.06
$\nu_7$	316	0	316	0.002
$\nu_8$	324	0	324	0.002
$\nu_9$	328	0	328	0.02
$\nu_{10}$	389	0	389	0.04

# Appendices



# Références bibliographiques

- [1] Morihisa Saeki, Hiroshi Akagi, and Masaaki Fujii. Theoretical study on the structure and the frequency of isomers of the naphthalene dimer. *Journal of chemical theory and computation*, 2(4):1176–1183, 2006.
- [2] KH Michaelian, Q Wen, BE Billinghamurst, JM Shaw, and V Lastovka. Far-and mid-infrared photoacoustic spectra of tetracene, pentacene, perylene and pyrene. *Vibrational Spectroscopy*, 58:50–56, 2012.
- [3] Elisabetta Venuti, Raffaele Guido Della Valle, Luca Farina, Aldo Brillante, Matteo Masino, and Alberto Girlando. Phonons and structures of tetracene polymorphs at low temperature and high pressure. *Physical Review B*, 70(10):104106, 2004.
- [4] RB Campbell, J Monteath Robertson, and J Trotter. The crystal structure of hexacene, and a revision of the crystallographic data for tetracene. *Acta crystallographica*, 15(3):289–290, 1962.
- [5] RB Campbell, J Monteath Robertson, and J Trotter. The crystal and molecular structure of pentacene. *Acta Crystallographica*, 14(7):705–711, 1961.
- [6] Christine C Mattheus, Anne B Dros, Jacob Baas, Auke Meetsma, Jan L de Boer, and Thomas TM Palstra. Polymorphism in pentacene. *Acta Crystallographica Section C: Crystal Structure Communications*, 57(8):939–941, 2001.
- [7] Daniel Holmes, Sriram Kumaraswamy, Adam J Matzger, and K Peter C Vollhardt. On the nature of nonplanarity in the [N] phenylenes. *Chemistry—A European Journal*, 5(11):3399–3412, 1999.
- [8] Theo Siegrist, Christian Kloc, Jan H Schön, Bertram Batlogg, Robert C Haddon, Steffen Berg, and Gordon A Thomas. Enhanced physical properties in a pentacene polymorph. *Angewandte Chemie International Edition*, 40(9):1732–1736, 2001.
- [9] Christine C Mattheus, Anne B Dros, Jacob Baas, Gert T Oostergetel, Auke Meetsma, Jan L de Boer, and Thomas TM Palstra. Identification of polymorphs of pentacene. *Synthetic metals*, 138(3):475–481, 2003.
- [10] Christine C Mattheus, Gilles A de Wijs, Robert A de Groot, and Thomas TM Palstra. Modeling the polymorphism of pentacene. *Journal of the American Chemical Society*, 125(20):6323–6330, 2003.
- [11] Axel D Becke. Density-functional thermochemistry. III. the role of exact exchange. *The Journal of chemical physics*, 98(7):5648–5652, 1993.

- [12] Chengteh Lee, Weitao Yang, and Robert G Parr. Development of the colle-salvetti correlation-energy formula into a functional of the electron density. *Physical review B*, 37(2):785, 1988.
- [13] Charles W Bauschlicher. A comparison of the accuracy of different functionals. *Chemical Physics Letters*, 246(1):40–44, 1995.
- [14] Julian Tirado-Rives and William L Jorgensen. Performance of B3LYP density functional methods for a large set of organic molecules. *Journal of Chemical Theory and Computation*, 4(2):297–306, 2008.
- [15] PJ Stephens, FJ Devlin, CFn Chabalowski, and Michael J Frisch. Ab initio calculation of vibrational absorption and circular dichroism spectra using density functional force fields. *The Journal of Physical Chemistry*, 98(45):11623–11627, 1994.
- [16] Charles W Bauschlicher and Stephen R Langhoff. The calculation of accurate harmonic frequencies of large molecules: the polycyclic aromatic hydrocarbons, a case study. *Spectrochimica Acta Part A: Molecular and Biomolecular Spectroscopy*, 53(8):1225–1240, 1997.
- [17] Neil Gohaud, Didier Begue, and Claude Pouchan. Vibrational spectra of methylolithium and its aggregates: a new interpretation from ab initio anharmonic calculations. *Chemical physics*, 310(1):85–96, 2005.
- [18] Sándor Kristyán and Péter Pulay. Can (semi) local density functional theory account for the london dispersion forces? *Chemical physics letters*, 229(3):175–180, 1994.
- [19] Pavel Hobza, Tomáš Reschel, et al. Density functional theory and molecular clusters. *Journal of computational chemistry*, 16(11):1315–1325, 1995.
- [20] Didier Begue, Stéphane Elissalde, Eve Pere, Pierre Iratcabal, and Claude Pouchan. New theoretical and experimental infrared results on formaldehyde in solution. *The Journal of Physical Chemistry A*, 110(25):7793–7800, 2006.
- [21] Didier Begue, Greg GuangHua Qiao, and Curt Wentrup. Nitrile imines: matrix isolation, IR spectra, structures, and rearrangement to carbodiimides. *Journal of the American Chemical Society*, 134(11):5339–5350, 2012.
- [22] J\_A Pople, R Krishnan, HB Schlegel, and J\_S\_ Binkley. Derivative studies in Hartree-Fock and Møller-Plesset theories. *International Journal of Quantum Chemistry*, 16(S13):225–241, 1979.
- [23] Grzegorz Chalasinski and Małgorzata. M Szczęśniak. State of the art and challenges of the ab initio theory of intermolecular interactions. *Chemical reviews*, 100(11):4227–4252, 2000.
- [24] Erin R Johnson and Gino A DiLabio. Structure and binding energies in van der waals dimers: Comparison between density functional theory and correlated ab initio methods. *Chemical physics letters*, 419(4):333–339, 2006.
- [25] Andrzej Eilmes. A theoretical study of small tetracene clusters: Stability and charge stabilization energies. *Computational and Theoretical Chemistry*, 982:25–29, 2012.

- [26] Jeng-Da Chai and Martin Head-Gordon. Systematic optimization of long-range corrected hybrid density functionals. *The Journal of chemical physics*, 128(8):084106, 2008.
- [27] Ulrike Salzner and Aykut Aydin. Improved prediction of properties of  $\pi$ -conjugated oligomers with range-separated hybrid density functionals. *Journal of chemical theory and computation*, 7(8):2568–2583, 2011.
- [28] RBJS Krishnan, J Stephen Binkley, Rolf Seeger, and John A Pople. Self-consistent molecular orbital methods. XX. a basis set for correlated wave functions. *The Journal of Chemical Physics*, 72(1):650–654, 1980.
- [29] Michael J Frisch, John A Pople, and J Stephen Binkley. Self-consistent molecular orbital methods 25. supplementary functions for gaussian basis sets. *The Journal of chemical physics*, 80(7):3265–3269, 1984.
- [30] Georg Kresse and Jürgen Furthmüller. Efficient iterative schemes for ab initio total-energy calculations using a plane-wave basis set. *Physical review B*, 54(16):11169, 1996.
- [31] John P Perdew, Kieron Burke, and Matthias Ernzerhof. Generalized gradient approximation made simple. *Physical review letters*, 77(18):3865, 1996.
- [32] Stefan Grimme. Semiempirical gga-type density functional constructed with a long-range dispersion correction. *Journal of computational chemistry*, 27(15):1787–1799, 2006.
- [33] Stefan Grimme, Stephan Ehrlich, and Lars Goerigk. Effect of the damping function in dispersion corrected density functional theory. *Journal of computational chemistry*, 32(7):1456–1465, 2011.
- [34] Alexandre Tkatchenko and Matthias Scheffler. Accurate molecular van der waals interactions from ground-state electron density and free-atom reference data. *Physical review letters*, 102(7):073005, 2009.
- [35] Alexandre Tkatchenko, Robert A DiStasio Jr, Roberto Car, and Matthias Scheffler. Accurate and efficient method for many-body van der waals interactions. *Physical review letters*, 108(23):236402, 2012.
- [36] Max Dion, Henrik Rydberg, Elsebeth Schröder, David C Langreth, and Bengt I Lundqvist. Van der waals density functional for general geometries. *Physical review letters*, 92(24):246401, 2004.
- [37] Roberto Dovesi, Roberto Orlando, Alessandro Erba, Claudio M Zicovich-Wilson, Bartolomeo Civalleri, Silvia Casassa, Lorenzo Maschio, Matteo Ferrabone, Marco De La Pierre, Philippe D’Arco, et al. Crystal14: A program for the ab initio investigation of crystalline solids. *International Journal of Quantum Chemistry*, 114(19):1287–1317, 2014.
- [38] MJEA Frisch, GW Trucks, Hs B Schlegel, GE Scuseria, MA Robb, JR Cheeseman, G Scalmani, V Barone, B Mennucci, GAea Petersson, et al. Gaussian 09, revision a. 02, gaussian. Inc., Wallingford, CT, 2009.
- [39] Charles W Bauschlicher and Harry Partridge. The sensitivity of B3LYP atomization energies to the basis set and a comparison of basis set requirements for CCSD (T) and B3LYP. *Chemical physics letters*, 240(5):533–540, 1995.

- [40] Didier Bégué, Neil Gohaud, Claude Pouchan, Patrick Cassam-Chenaï, and Jacques Liévin. A comparison of two methods for selecting vibrational configuration interaction spaces on a heptatomic system: Ethylene oxide. *The Journal of chemical physics*, 127(16):164115, 2007.
- [41] Joel M Bowman, Tucker Carrington, and Hans-Dieter Meyer. Variational quantum approaches for computing vibrational energies of polyatomic molecules. *Molecular Physics*, 106(16-18):2145–2182, 2008.
- [42] D Bégué, I Baraille, PA Garrain, A Dargelos, and T Tassaing. Calculation of IR frequencies and intensities in electrical and mechanical anharmonicity approximations: Application to small water clusters. *The Journal of chemical physics*, 133(3):034102, 2010.
- [43] Neil Gohaud, Didier Begue, Clovis Darrigan, and Claude Pouchan. New parallel software (P\_Anhar) for anharmonic vibrational calculations: Application to  $(\text{CH}_3\text{Li})_2$ . *Journal of computational chemistry*, 26(7):743–754, 2005.
- [44] I Baraille, C Larrieu, A Dargelos, and M Chaillet. Calculation of non-fundamental IR frequencies and intensities at the anharmonic level. I. the overtone, combination and difference bands of diazomethane,  $\text{h}_2 \text{ cn}_2$ . *Chemical Physics*, 273(2):91–101, 2001.
- [45] Franco Cataldo, Giancarlo Angelini, D Aníbal García-Hernández, and Arturo Manchado. Far infrared (terahertz) spectroscopy of a series of polycyclic aromatic hydrocarbons and application to structure interpretation of asphaltenes and related compounds. *Spectrochimica Acta Part A: Molecular and Biomolecular Spectroscopy*, 111:68–79, 2013.
- [46] G Mallocci, G Mulas, G Cappellini, and C Joblin. Time-dependent density functional study of the electronic spectra of oligoacenes in the charge states- 1, 0,+ 1, and+ 2. *Chemical Physics*, 340(1):43–58, 2007.
- [47] Elisabetta Venuti, Raffaele Guido Della Valle, Aldo Brillante, Matteo Masino, and Alberto Girlando. Probing pentacene polymorphs by lattice dynamics calculations. *Journal of the American Chemical Society*, 124(10):2128–2129, 2002.
- [48] A Brillante, RG Della Valle, L Farina, A Girlando, M Masino, and E Venuti. Raman phonon spectra of pentacene polymorphs. *Chemical physics letters*, 357(1):32–36, 2002.
- [49] C Pratt Brock and JACK D Dunitz. Temperature dependence of thermal motion in crystalline naphthalene. *Acta Crystallographica Section B: Structural Crystallography and Crystal Chemistry*, 38(8):2218–2228, 1982.
- [50] Julio C Facelli and David M Grant. Determination of molecular symmetry in crystalline naphthalene using solid-state NMR. 1993.
- [51] C Pratt Brock and JD Dunitz. Temperature dependence of thermal motion in crystalline anthracene. *Acta Crystallographica Section B: Structural Science*, 46(6):795–806, 1990.
- [52] M Hineno and H Yoshinaga. Far-ir spectra of napthalene, anthracene, biphenyl, diphenyl ether, diphenylamine, diphenyl sulfoxide, and benzophenone at liquid helium temperature. *Spectrochimica Acta Part A: Molecular Spectroscopy*, 31(5):617–620, 1975.

- [53] Seiji Tsuzuki, Kazumasa Honda, Tadafumi Uchimaru, and Masuhiro Mikami. High-level ab initio computations of structures and interaction energies of naphthalene dimers: Origin of attraction and its directionality. *The Journal of chemical physics*, 120(2):647–659, 2004.
- [54] TR Walsh. An ab initio study of the low energy structures of the naphthalene dimer. *Chemical physics letters*, 363(1):45–51, 2002.
- [55] Miroslav Rubeš, Ota Bludský, and Petr Nachtigall. Investigation of the benzene–naphthalene and naphthalene–naphthalene potential energy surfaces: DFT/CCSD (T) correction scheme. *ChemPhysChem*, 9(12):1702–1708, 2008.
- [56] SF Boys and F Bernardi. The calculation of small molecular interactions by the differences of separate total energies. some procedures with reduced errors. *Molecular Physics*, 100(1):65–73, 2002.
- [57] Edward G Hohenstein and C David Sherrill. Density fitting and cholesky decomposition approximations in symmetry-adapted perturbation theory: Implementation and application to probe the nature of  $\pi$ – $\pi$  interactions in linear acenes. *The Journal of Chemical Physics*, 132(18):184111, 2010.
- [58] EP Krainov. The vibrational spectra of aromatic compounds. xix. calculation and interpretation of the vibrational spectra of Naphthalene and some Deuterionaphthalenes. *Opt. Spectr. (USSR)(English Transl.)*, 16, 1964.
- [59] Stefan Grimme. Do special noncovalent  $\pi$ – $\pi$  stacking interactions really exist? *Angewandte Chemie International Edition*, 47(18):3430–3434, 2008.
- [60] Brant Billinghurst, Tim May, Les Dallin, Ward Wurtz, Mark de Jong, and Kirk H Michaelian. Photoacoustic spectroscopy using coherent synchrotron radiation: application to  $\alpha$ -lactose monohydrate. *Optics letters*, 35(18):3090–3092, 2010.
- [61] S Appalakondaiah, G Vaitheeswaran, and S Lebègue. Dispersion corrected structural properties and quasiparticle band gaps of several organic energetic solids. *The Journal of Physical Chemistry A*, 119(24):6574–6581, 2015.
- [62] Evert Jan Meijer and Michiel Sprik. A density-functional study of the intermolecular interactions of benzene. *The Journal of chemical physics*, 105(19):8684–8689, 1996.
- [63] Andrzej Katrusiak, Marcin Podsiadło, and Armand Budzianowski. Association ch...  $\pi$  and no van der waals contacts at the lowest limits of crystalline benzene i and ii stability regions. *Crystal Growth & Design*, 10(8):3461–3465, 2010.
- [64] Francesca PA Fabbiani, David R Allan, Simon Parsons, and Colin R Pulham. Exploration of the high-pressure behaviour of polycyclic aromatic hydrocarbons: naphthalene, phenanthrene and pyrene. *Acta Crystallographica Section B: Structural Science*, 62(5):826–842, 2006.
- [65] U Sondermann, A Kutoglu, and H Bassler. X-ray diffraction study of the phase transition in crystalline tetracene. *The Journal of Physical Chemistry*, 89(9):1735–1741, 1985.

- [66] DM Burns and J Iball. Refinement of the structure of chrysene. In *Proceedings of the Royal Society of London A: Mathematical, Physical and Engineering Sciences*, volume 257, pages 491–514. The Royal Society, 1960.
- [67] VK Belsky, VE Zavodnik, and VM Vozzhennikov. Fluorene, c13h10. *Acta Crystallographica Section C: Crystal Structure Communications*, 40(7):1210–1211, 1984.
- [68] Robert Kalescky, Elfi Kraka, and Dieter Cremer. Description of aromaticity with the help of vibrational spectroscopy: Anthracene and phenanthrene. *The Journal of Physical Chemistry A*, 118(1):223–237, 2013.
- [69] A Bree and RA Kydd. Infrared spectrum of anthracene crystals. *The Journal of Chemical Physics*, 48(12):5319–5325, 1968.
- [70] Faustine Spillebout, Didier Begue, Isabelle Baraille, and John M Shaw. On discerning intermolecular and intramolecular vibrations in experimental acene spectra. *Energy & Fuels*, 28(5):2933–2947, 2014.
- [71] J Godec and L Colombo. Interpretation of the vibrational spectrum of crystalline phenanthrene. *The Journal of Chemical Physics*, 65(11):4693–4700, 1976.
- [72] A Bree, FG t Solven, and VVB Vilkos. A vibrational analysis for phenanthrene. *Journal of Molecular Spectroscopy*, 44(2):298–319, 1972.
- [73] KH Michaelian, BE Billinghamurst, JM Shaw, and V Lastovka. Far-infrared photoacoustic spectra of tetracene, pentacene, perylene and pyrene. *Vibrational Spectroscopy*, 49(1):28–31, 2009.
- [74] K Zhang, B Guo, P Colarusso, and PF Bernath. Far-infrared emission spectra of selected gas-phase pahs: Spectroscopic fingerprints. *Science*, 274(5287):582, 1996.
- [75] KH Michaelian, SA Oladepo, JM Shaw, X Liu, D Bégué, and I Baraille. Raman and photoacoustic infrared spectra of fluorene derivatives: Experiment and calculations. *Vibrational Spectroscopy*, 74:33–46, 2014.
- [76] TD Klots and WB Collier. Vibrational spectra, structure, assignment, and ideal-gas thermodynamics of a three-ring molecule: dibenzofuran. *Journal of molecular structure*, 380(1):1–14, 1996.
- [77] Tomáš Bučko, S Lebègue, Jürgen Hafner, and JG Ángyán. Tkatchenko-scheffler van der waals correction method with and without self-consistent screening applied to solids. *Physical Review B*, 87(6):064110, 2013.